Atmospheric Pollution Research 15 (2024) 101987

Contents lists available at ScienceDirect

Atmospheric Pollution Research

journal homepage: www.elsevier.com/locate/apr

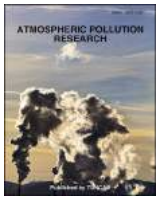

Unveiling the air pollution tapestry in China: A comprehensive assessment of spatiotemporal variations through geographically and temporally weighted regression

Xuchu Yang [a], Yi Yang [a,*], Shenghua Xu [a,b], Hamed Karimian [a,**], Yangyang Zhao [b], Lingbo Jin [a], Yanchang Xu [a], Yanli Qi [c]

[a] School of Marine Technology and Geomatics, Jiangsu Ocean University, Lianyungang, 222005, China
[b] Research Center of Geospatial Big Data Application, Chinese Academy of Surveying and Mapping, Beijing, 100830, China
[c] Institute of Transportation Studies, University of California, Davis, USA

ARTICLE INFO

Keywords:
Urban air pollutants
Air quality
Spatiotemporal correlation
Spatial distribution
China
GTWR

ABSTRACT

Study of air pollution informs environmentally-conscious policies and urban planning by government and businesses, leading to more scientific decision-making. This paper comprehensively analyzes the spatiotemporal correlation of six air pollutants ($PM_{2.5}$, PM_{10}, SO_2, NO_2, CO, and O_3) at the national level of China from 2015 to 2021. The temporal changes in environmental air pollutants are examined through statistical data analysis. Secondly, the annual and quarterly spatial distribution characteristics of air pollutants are analyzed by utilizing global and local spatial autocorrelation analysis and visualizing pollutant concentration data. To quantify the spatiotemporal correlation information obtained from the data, we proposed a novel framework based on the Geographically and Temporally Weighted Regression (GTWR) model to provide a local approach for detecting the spatiotemporal correlation between urban air pollutants on a large scale. The framework's experimental results showed that the significant correlation between urban air pollutants in time and space ranged from 0.45 to 0.9, which is better than traditional correlation algorithm, and the degree of local spatiotemporal correlations can be explained by spatiotemporal coefficients. We find noticeable differences in the correlations between different pollutants and geographical boundaries in the spatial dimension. Furthermore, in terms of spatiotemporal location, $PM_{2.5}$, PM_{10}, NO_2, SO_2, and CO exhibit positive correlations with each other, while O_3 shows both positive and negative correlations with other pollutants. This study offers an important reference for air quality monitoring and prediction, contributing to the improvement of accuracy and timeliness of air quality warnings.

1. Introduction

Air quality is a critical aspect of human life. According to the World Health Organization (WHO), air quality in most parts of the world fails to meet the organization's limits and standards. This alarming statistic has been associated with an estimated 7 million premature deaths each year due to air pollution (Ouyang et al., 2022). Environmental issues are crucial these days and providing studies to solve these issues attracted scholars in different fields (Cai et al., 2017; Guan et al., 2019b; Liu et al., 2020). In response to this global issue, the WHO has established new guidelines for six pollutants, namely carbon monoxide (CO), nitrogen dioxide (NO_2), ozone (O_3), inhalable particulate matter with diameters of 10 μm or less (PM_{10}), fine particulate matter with diameters of 2.5 μm or less ($PM_{2.5}$), and sulfur dioxide (SO_2). These pollutants are also considered key indicators of air quality under China's latest ambient air standard, GB3095-2012. Exposure to these pollutants has been linked to a range of adverse health effects. Specifically, they can exacerbate chronic respiratory conditions (Chen et al., 2022b; Mariscal-Aguilar et al., 2023; Pompilio and Di Bonaventura, 2020) and cardiovascular diseases (Karimian et al., 2023). Moreover, they have been found to weaken the immune system, damage lung tissue, and even contribute to premature death and cancer (Liao et al., 2022). Exposure to pollutants

Peer review under responsibility of Turkish National Committee for Air Pollution Research and Control.
* Corresponding author.
** Corresponding author.
E-mail addresses: yangyi@jou.edu.cn (Y. Yang), hamedk@pku.edu.cn (H. Karimian).

https://doi.org/10.1016/j.apr.2023.101987
Received 5 August 2023; Received in revised form 10 November 2023; Accepted 10 November 2023
Available online 15 November 2023

such as carbon monoxide (CO), sulfur dioxide (SO_2), and nitrogen dioxide (NO_2) has been associated with reduced work capacity, worsened cardiovascular conditions, impaired lung function, respiratory diseases, lung irritation, and alterations in lung defense systems (McKeon et al., 2022; Ryter et al., 2018).

In recent decades, machine learning-based approaches have shown their feasibility in extracting the trends between variables (Guan et al., 2019a; Qiu et al., 2020). In order to gain a deeper understanding of the interactions and effects of various pollutants and effectively evaluate and address environmental pollution issues, previous studies have extensively explored the correlation of air pollution. For instance, Filonchyk et al. (2018) analyzed the linear correlation of major air pollutants in Lanzhou, Gansu Province, and found that there was a strong correlation between $PM_{2.5}$ and PM_{10}. They concluded that reducing PM_{10} emissions is crucial for decreasing particulate matter pollution and improving China's air quality. To investigate the correlation of pollutants on a larger scale, Kuerban et al. (2020) examined six types of urban pollutants in China from 2015 to 2018. They divided the pollutants into seven major geographical regions, including northwest, north China, northeast, Qinghai-Tibet Plateau, southeast, and southwest, to explore their individual correlations. In addition, Zhao et al. (2021) conducted a study on AQI and six types of urban pollutants in China from 2014 to 2019. They selected 14 representative cities as study objects to investigate correlations within the cities, refining the research scale while increasing the workload. Although some studies have analyzed the correlation of urban pollutants in China, such as the study by (Wang et al., 2022a), they have limitations when it comes to reflecting correlations at the urban scale. These studies often consider only the global influence, overlooking important aspects such as spatiotemporal location.

Urban ambient air pollution exhibits spatial diffusion in regional space, leading to interaction and spatial correlation between different cities. Differences in industrial structure, population size, and emission sources (Karimian et al., 2019) among cities result in significant variations in the characteristics of urban air composite pollution, giving rise to substantial spatial non-stationarity. Statistical analysis is indispensable to uncover the objective laws governing the distribution and generation of air quality pollution, with regression analysis serving as an essential analytical tool. Additionally, urban air pollution concentration undergoes marked seasonal changes (Wang et al., 2021). While deep learning models have demonstrated their potential for predicting pollutant concentrations (He et al., 2022; Tan et al., 2022), it is important to note that they tend to be computationally intensive and often lack the capability to offer detailed surface distributions of air pollutants. Traditional statistical methods have advantages in revealing objective patterns and explaining the causes of air pollution distribution. These methods are built on a solid theoretical foundation and provide statistically significant and interpretable model parameters. Brunsdon et al. (1996) and Huang et al. (2010) have proposed the Geographically Weighted Regression (GWR) model and Geographically and Temporally Weighted Regression (GTWR) model. Despite the challenges of large and insufficient sample data sets covering a wide area, the spatiotemporal regression model can simultaneously integrate time or spatial heterogeneity to detect potential information through the spatiotemporal weighting mechanism (He and Huang, 2018). They have been proven to be valuable in understanding causal relationships, making inferences, and interpreting results (Guo et al., 2017; Jiang et al., 2023; Shen et al., 2022; Xu et al., 2023).

Chu et al. (2015) established the relationship between $PM_{2.5}$ and PM_{10} using GTWR model, providing valuable information for planners to better understand the spatiotemporal heterogeneity of particulate matter and the relationship between $PM_{2.5}$ and PM_{10}. However, there are two regrets in the above research. One is that the pure connection between pollutants is not considered separately. The other is that the research area is too small and may not represent the social situation of the entire country or a larger region. This study reinforces existing knowledge and provides a theoretical basis for further research on the six types of urban air pollutants in China.

Since 2013, the Chinese government has made significant efforts in the development of automated monitoring stations to track air quality. The China National Environmental Monitoring Centre has made data available to the public for six air quality indicators, collected from high-density monitoring stations across the country. Utilizing this data, along with surface observations, high-resolution air quality reanalysis datasets for China have been constructed. In comparison to the European Centre for Medium Range Weather Forecasts' (ECWMF) Copernicus Atmospheric Monitoring Service Reanalysis (CAMSRA) dataset, China's dataset demonstrates higher precision in measuring surface gaseous pollutants nationwide (Kong et al., 2021). This comprehensive dataset provides essential data support for the analysis conducted in this study.

The objectives of this study can be categorized into two primary aims. Firstly, we aim to conduct a comprehensive statistical analysis of urban air pollutants in Chinese cities, with a focus on identifying temporal patterns to understand how pollution levels change over time. Additionally, we intend to explore the spatial distribution of urban air pollutants in Chinese cities using the Moran's I, shedding light on geographical disparities in air quality and providing insights into how pollution varies across different regions. To enhance our understanding further, we will employ visualization techniques to depict the variations in air pollution concentrations across different cities. Secondly, our study delves into the spatial correlations of urban air pollution in China. We leverage advanced spatial regression analysis methods, including the Ordinary Least Squares (OLS) and Geographical Weighted Regression (GWR) models, to unravel the complex web of spatial interdependencies among various pollutants, providing valuable insights into their relationships. Furthermore, we employ the Geographically and Temporally Weighted Regression (GTWR) model to investigate the influence of spatiotemporal changes, which enables us to establish a robust spatiotemporal relationship between pollutants and understand how these relationships evolve over time.

The rest of this paper is organized as follows: the second section provides a brief description of the data processing procedures, as well as the analytical methods and principles utilized in this study. The third section presents the experimental results to reveal the spatiotemporal variation and correlations of urban air pollutants, and provides an interpretation and discussion of the findings. The fourth section summarizes conclusions of this study. Fig. 1 illustrates the analytical framework for the spatiotemporal correlation analysis of urban air pollutants.

2. Materials and methods

2.1. Study area and data

China is located on the west coast of the Pacific Ocean in eastern Asia, spanning approximately 3°86' - 53°55′ north latitude and 73°66' - 135°05′ east longitude. It boasts a vast territory, covering a total land area of about 9.6 million square kilometers, making it the third-largest country in the world, following Russia and Canada. In recent years, China's economy has experienced rapid growth to cater to the increasing material and cultural demands of its population. However, this growth has come at a cost, leading to various challenges. These challenges include the continued reliance on non-renewable energy sources, the necessity to optimize the industrial structure, the urgent need to accelerate urban transportation development, and the relatively delayed efforts in preventing and controlling air pollution. Consequently, these problems have resulted in increasingly severe urban air pollution and a decline in air quality.

This study utilizes open-source data collected from 1497 monitoring sites across China from China National Environmental Monitoring Centre (CNEMC, http://www.cnemc.cn) between 2015 and 2021. The sites are visually represented in Fig. 2, highlighting specific geographical

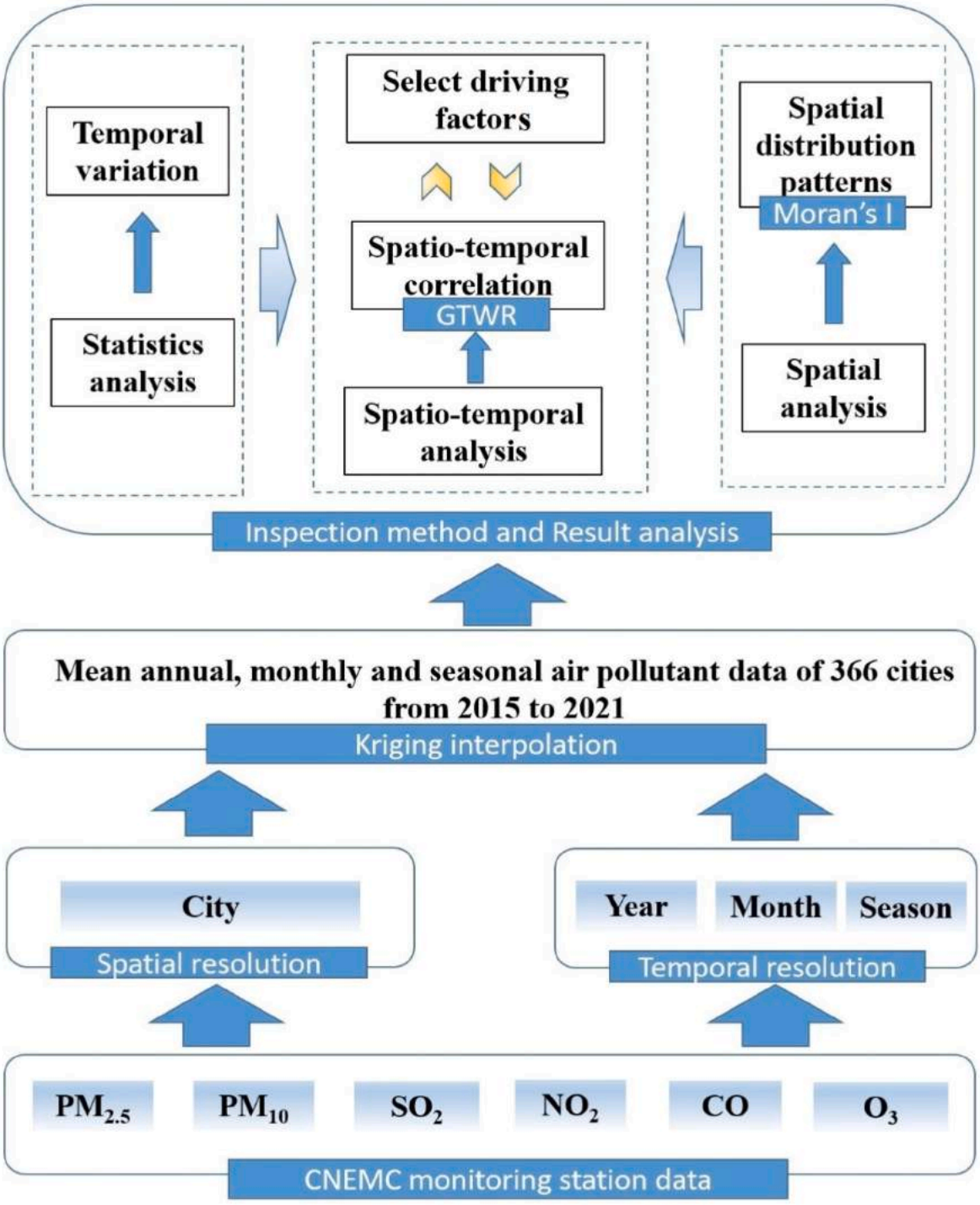

Fig. 1. Analytical framework for spatiotemporal correlation of urban air pollutants.

boundaries. China divides its territory into seven major geographical regions based on provincial-level administrative divisions, aiming to facilitate research and management in various aspects such as geography, human history, climate, economy, and administrative governance. Notably, the Heihe-Tengchong line (HT line, straight line) and the Qinling-Huaihe line (QH line, dashed line) are depicted. These lines serve as contrasting dividers; the HT line divides the population density of China, while the QH line separates the northern and southern regions of China geographically by the Qinling Mountains and the Huaihe river. The data includes measurements of $PM_{2.5}$, PM_{10}, NO_2, SO_2, CO, and O_3. To standardize the data, the 24-h average monitoring concentration of pollutants at all stations within a city is employed to represent urban pollutants. Additionally, the monitoring concentration of O_3 pollutants is substituted with an 8-h average. Daily average pollutant concentrations are calculated for cities above the prefecture level and provinces directly under the jurisdiction of county-level cities. Monthly averages are computed to ensure temporal continuity. To address missing urban pollution concentration data, ordinary kriging interpolation is employed. This interpolation technique fills in the gaps, resulting in monthly data for 366 Chinese cities from 2015 to 2021. It is worth mentioning that our data are normally distributed.

Previous studies (Cao et al., 2020; Han et al., 2020; Karimian et al.,

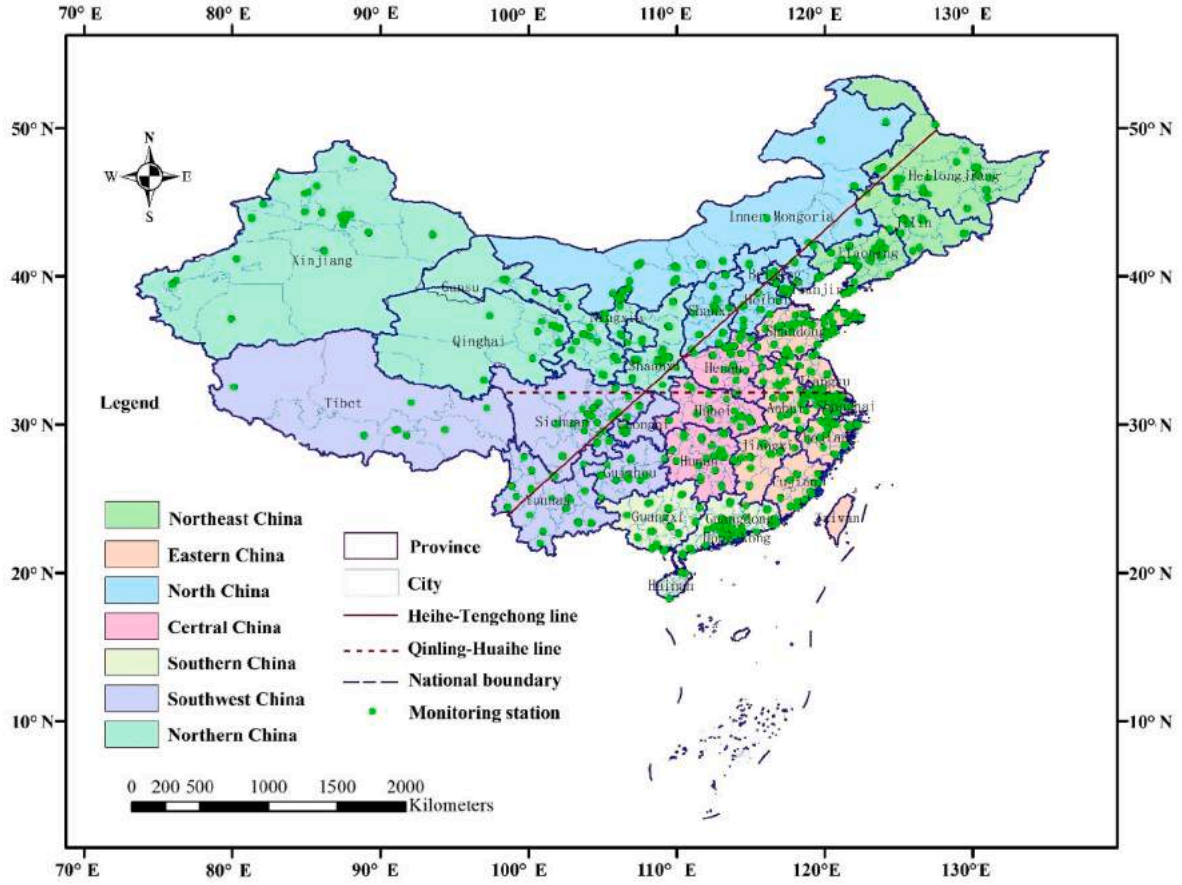

Fig. 2. Study area and location of air pollution monitoring stations in China.

2017) have demonstrated that terrain, human activities, and meteorological conditions can have varying impacts on the concentration of urban air pollutants. In this study, we aim to investigate these impacts further. To assess the influence of terrain, we obtained terrain data from the Resource and Environment Science Data Centre of the Chinese Academy of Sciences (https://www.resdc.cn). Utilizing ArcGIS "3D analyst tools-raster surface-slope/aspect" and "Spatial analyst tools-zonal-zonal statistics as table," we calculated the surface evolution and terrain fluctuation of different cities. To analyze the impact of weather changes, relevant meteorological data was sourced from the China Meteorological Centre (http://data.cma.cn/). This data will provide valuable insights into the meteorological conditions during the study period. Moreover, we incorporated urban green coverage and population density data from the China City Statistical Yearbook (http://www.stats.gov.cn/sj/ndsj) to account for the influence of human activities. In cases where data was missing, we supplemented it with information from the China County Statistical Yearbook. By utilizing these comprehensive datasets, we aim to support and validate our research thesis.

2.2. Spatial distribution pattern and autocorrelation

Urban ambient air pollution is dispersed across regional space, leading to interactions between different cities and exhibiting spatial correlation. To assess the overall distribution pattern and spatial correlation of air quality at the urban scale, we employed the global autocorrelation method. The Global Moran's I was utilized as the test model for this purpose.

$$I^{Global} = \frac{n\sum_{i=1}^{n}\sum_{j=1}^{n} W_{ij}(x_i-\bar{x})(x_j-\bar{x})}{\left(\sum_{i=1}^{n}\sum_{j=1}^{n} W_{ij}\right)\sum_{i=1}^{n}(x_i-\bar{x})^2}, (i\neq j) \quad (1)$$

In the calculation of Moran's I, n is the total number of observation points, the attribute values of urban air pollutants for the ith and jth urban points are denoted as x_i and x_j, respectively. The symbol $\bar{x}$ represents the mean value of the current pollutant across all urban points. The matrix W_{ij} represents the spatial weight between cities i and j, taking a value of 1 if the cities are adjacent and 0 if they are separate. The total number of sample cities is denoted as n. When the value of Moran's I is positive, it indicates that urban air pollution in the study area exhibits an agglomeration distribution state. The closer the value is to 1, the more significant the agglomeration of air pollution is. To capture the clustering or dispersion of spatial pollution between cities and identify the geographical locations of such patterns, the application of local spatial autocorrelation is essential. Local spatial autocorrelation analysis allows us to examine the relationship between each observation point and its surrounding environment. One commonly used measure for local spatial autocorrelation is the Local Moran's I. The formula for calculating the Local Moran's I is as follows:

$$I_i^{Local} = \frac{x_i-\bar{x}}{\frac{1}{n}\sum_{i=1}^{n}(x_i-\bar{x})}\sum_{i\neq j}^{n} W_{ij}(x_j-\bar{x}) \quad (2)$$

where I_i^{Local} represent the local Moran's I for the observation at point i. x_i is the attribute value of the pollution at point i. $\bar{x}$ is the mean of the pollution attribute across all points. W_{ij} is the spatial weight between points i and j. n is the total number of observation points. The meaning of

the I_i^{Local} is similar to that of I^{Global}, where an index greater than 0 indicates that the high/low values of region i are surrounded by high or low values, respectively; Less than 0 the table shows that the high/low values of domain i are surrounded by the low/high values of the circumference.

2.3. Geographically and temporally weighted regression model

The variation in the pollution levels of urban air quality is influenced by different geographical locations. The traditional global OLS model encounters challenges in capturing the spatial heterogeneity of regional coefficients and identifying local features between explanatory and response variables. Given the diverse characteristics of urban air pollution, including variations in industrial structure, population size, and emission sources across cities, there exists significant spatial non-stationarity. To address these issues, the GWR model incorporated spatial weights to achieve localized regression within the study region and effectively captures heterogeneous information across different areas. At present, it also has high practical value (Comber et al., 2023). Moreover, the GTWR model had introduced to consider both temporal and spatial dimensions by incorporating time and latitude information (Wang et al., 2022b). It is important to acknowledge that geographical processes exhibit non-stationary spatial and temporal characteristics, and spatial latitude significantly influences air pollution. Additionally, the temporal dimension, such as seasonal variations, is an essential attribute since air pollution concentrations vary greatly across different seasons (Wang et al., 2021). By employing models like GWR and GTWR, we can better account for the spatial and temporal complexities of urban air pollution, capturing the localized effects and addressing the spatial heterogeneity of the phenomena.

To gain a deeper understanding of the complex relationships between urban air pollutants, it is important to investigate their pairwise interactions. This can be achieved by employing the GTWR model, which allows us to establish the relationship between two pollutants, such as $PM_{2.5}$ and PM_{10}. The GTWR model is defined by the following formula:

$$y_i = \beta_{i0}(u_i, v_i, t_i) + \beta_{i1}(u_i, v_i, t_i)x_i + \varepsilon_i, i = 1, 2, 3 \ldots n \tag{3}$$

Where y_i represents the dependent variable (e.g., $PM_{2.5}$ concentration) at location i. x_i represents the independent variable (e.g., NO_2 concentration) at location i. β_{i0} is the spatially varying intercept. β_{i1} is the spatially varying coefficient for the independent variable. ε_i is the error term. n represents the total number of observation points. The GTWR model captures the spatial and temporal variations in the relationship between the two pollutants. It allows for the estimation of spatially varying coefficients, recognizing that the strength and direction of the relationship may differ across locations. This approach provides a more comprehensive and localized understanding of the association between $PM_{2.5}$ and PM_{10}.

The weighted least squares estimation approach is conducted by GTWR, where β_i represents $\beta_{i0}(u_i, v_i, t_i), \beta_{i1}(u_i, v_i, t_i)$. w_{ij} is spatiotemporal weight of the distance between the current city point i and other affected city points j.

Then $\widehat{\beta}_i = [\beta_{i0}, \beta_{i1}]^{\mathrm{T}}$, $W_i = diag(w_{i1}, w_{i2}, w_{i3}, \ldots, w_{in,})$, the ith regression coefficients $\widehat{\beta}_i$ is estimated :

$$\widehat{\beta}_i = \left(X^{\mathrm{T}} W_i X\right)^{-1} X^{\mathrm{T}} W_i y \tag{4}$$

Where X is the form of independent variable(s) matrix, n by two. W_i is calculated based on a specified kernel function and bandwidth. The most widely used kernel functions for spatial analysis are the Bisquare and Gaussian functions, with other functions such as Inverse Distance Weighting (IDW) also available. The equations for the Bisquare and Gaussian kernel functions are given by:

$$w_{ij} = exp\left[-\left(\frac{d_{ij}^{st}}{h}\right)^2 \right] \tag{5}$$

$$w_{ij} = \begin{cases} \left[1 - \left(\frac{d_{ij}^{st}}{h}\right)^2\right]^2 & d_{ij} \le h \\ 0 & d_{ij} > h \end{cases} \tag{6}$$

Where d_{ij}^{st} extend spatial distance in GWR is some measure of the spatiotemporal distance between the current city points i and other affected city points j. In real life, human perception of the earth is a plane. Latitude and longitude coordinates are obtained, which makes it necessary to convert to the Cartesian coordinate system to calculate Euclidean distance for more meeting the needs of reality.

The bandwidth parameter, denoted as h, plays a crucial role in the GTWR. It represents the non-negative decaying relationship between weights and distance in the model. The selection of an appropriate bandwidth is essential to ensure the accuracy of the GTWR estimation. When the bandwidth is too large, it includes points that have little influence on the estimation result. This can result in a loss of precision and potentially obscure the true relationships between variables. On the other hand, if the bandwidth is too small, the estimation result may suffer from overfitting, where the model fits the data too closely and fails to generalize well to new observations. To select an appropriate bandwidth, various methods are available, including the Cross-Validation (CV) method and the Akaike Information Criterion (AIC) method. The CV method involves dividing the dataset into training and validation subsets and assessing the model's performance using different bandwidth values. The bandwidth that yields the best predictive performance on the validation subset is selected. The AIC method aims to find the bandwidth that balances model fit and complexity by penalizing models with larger bandwidths. The bandwidth that minimizes the AIC value is typically chosen. Both the CV and AIC methods provide systematic approaches to select the optimal bandwidth for GTWR estimation, taking into account the trade-off between model complexity and predictive performance.

Following Eqs. (6) and (7), spatiotemporal distance d_{ij}^{st} replaces the spatial distance. The rationality is verified by the derivation of GWR weight. Therefore, we have following:

$$\left(d_{ij}^{st}\right)^2 = \lambda\left[\left(u_i - u_j\right)^2 - \left(v_i - v_j\right)^2\right] \divideontimes \mu\left(t_i - t_j\right)^2 \tag{7}$$

Where λ, μ are the scaling factors for time and space distances, respectively. ※ acts as an operator to integrate the relationship between the two. Here , Huang et al. proposed that the combination of them can effectively improve the accuracy of the model, then the formula for the hypothesis that the experiment holds is defined as:

$$\left(d_{ij}^{st}\right)^2 = \left[\left(u_i - u_j\right)^2 - \left(v_i - v_j\right)^2\right] + \tau\left(t_i - t_j\right)^2 \tag{8}$$

Where τ take the place of the λandμ, simplifying the calculation while bringing the same training effect.

The relationship between correlation and regression can be described as follows. Correlation measures the degree of association or closeness between two variables, indicating the strength and direction of their linear relationship. It assesses the extent to which changes in one variable are related to changes in another variable. On the other hand, regression analysis measures the impact of an independent variable on a dependent variable, aiming to establish a mathematical relationship that can predict or explain the variation in the dependent variable based on the independent variable.

In the study of environmental air pollution correlation, traditional correlation algorithms typically evaluate the correlation between major urban air pollutants without considering the mutual interaction of

geographical spatial location and time variation. To address this limitation, the classical and effective local spatiotemporal regression analysis method, namely the GTWR model, is adopted. This model allows for the measurement of the impact of urban air pollutants, such as PM_{10} on $PM_{2.5}$, PM_{10} on O_3, PM_{10} on NO_2, on each other at specific spatiotemporal locations. In this context, the GTWR model enables the calculation of the statistical R^2 index to represent the correlation between these pollutants. The R^2 index measures the proportion of variation in the dependent variable (e.g., $PM_{2.5}$, O_3, or NO_2) that can be explained by the independent variable (e.g., PM_{10}) in the GTWR model. The spatiotemporal coefficient in the GTWR model serves as an evaluation index for the degree of local fitting. It indicates how the relationship between the variables varies across different locations and time periods. By estimating the spatiotemporal coefficients, one can assess the positive or negative correlation between the urban air pollutants. The R^2 index can be expressed by the following formula:

$$R^2 = 1 - \frac{\sum_{i=1}^{n}(y_i - \hat{y}_i)^2}{\sum_{i=1}^{n}(y_i - \bar{y}_i)^2} \quad (9)$$

The implementation stages of GTWR model are illustrated in Fig. 3.

3. Results and discussion

In this section, the statistical description is presented in charts and tables. Then, both global and local spatial autocorrelation were considered to explore the spatial patterns and clustering of the six major urban air pollutants in China. Furthermore, OLS Regression and GWR models are utilized to study spatial correlations, while the GTWR model is employed to investigate the impact of spatiotemporal variations.

3.1. Statistical description

Table .1 presents the percentage of days, from 2015 to 2021, in which the air pollution level exceeded the national second-level (unhealthy for sensitive groups). The maximum concentrations in the second level are 75 μg/m^3 for $PM_{2.5}$, 150 μg/m^3 for PM_{10}, 150 μg/m^3 for SO_2, 80 μg/m^3 for NO_2, 4 mg/m^3 for CO, and 160 μg/m^3 for O_3. The results revealed that $PM_{2.5}$ and PM_{10} are the main reason for air pollution level exceeds the second level with 10.14% and 7.1 % of the total city days, respectively, with the most severe pollution occurring during winter. Similarly, SO_2, NO_2, and CO also exhibit significant winter pollution, while O_3 displays higher pollution levels during summer.

To compare the annual and monthly variations of different pollutants, we analyzed the range of concentration and changes in average values using box plots. Our findings indicate that various pollutants, including $PM_{2.5}$, PM_{10}, SO_2, NO_2, and CO, have shown a decreasing trend under policy governance (Fig. 4). During the 2022 World Environment Day national event, Minister Huang of the Ministry of Ecology and Environment stated that the average concentration of $PM_{2.5}$ in cities at or above the prefecture level in China had decreased by 34.8% in 2021 compared to 2015. The research data presented in this paper is consistent with that statement, showing a decrease of 37.9% in the annual average concentration of $PM_{2.5}$ in cities at or above the prefecture level in China. Similarly, the concentrations of other pollutants have also decreased: PM_{10}, SO_2, NO_2, and CO decreased by 28.0%, 64.4%, 19.0%, and 37.4%, respectively. However, the concentration of O_3 exhibited a fluctuating state, with a 9% increase. Studies have shown that the increase in particulate matter can inhibit the rise of O_3 concentration, and the significant reduction in particulate pollution from 2015 to 2021 is likely a contributing factor to the increase in O_3 concentration. The monthly trend changes of various pollutants exhibit nonlinear patterns. $PM_{2.5}$, PM_{10}, SO_2, CO, and NO_2 show a negative correlation with O_3, with the former being more severe during winter pollution and the latter exhibiting higher concentrations during the summer (Fig. 5).

Table 1
The proportion of days in which pollutants exceed the limit.

Pollutant	Entire Year	Spring	Summer	Autumn	Winter
$PM_{2.5}$	10.14%	1.85%	0.35%	1.88%	6.08%
PM_{10}	7.07%	2.03%	0.30%	1.28%	3.47%
SO_2	0.18%	0.01%	0.00%	0.02%	0.15%
NO_2	0.86%	0.08%	0.00%	0.17%	0.61%
CO	0.18%	0.08%	0.00%	0.01%	0.15%
O_3	0.31%	0.09%	0.20%	0.01%	0.00%

3.2. Spatial patterns and cluster analyses

This study focuses on Chinese cities at or above the prefecture level and utilizes Moran's I to detect the spatial clustering of urban air pollutants. This analysis helps to gain a better understanding of the distribution characteristics of urban air pollutants, including the degree and extent of clustering, which is crucial for formulating environmental planning and decision-making. The Global Moran's I chart for various pollutants from 2015 to 2021 indicates significant clustering of environmental air pollution among regional cities in China (Table 2a). Upon observing the chart, it can be noted that Moran's I remained relatively stable from 2015 to 2019, but exhibited significant fluctuations from 2020 to 2021. This fluctuation could be attributed to the impact of lockdown measures during the fight against the epidemic, which resulted in inconsistent activities among cities and a decrease in the coefficient value. The clustering of particulate matter significantly decreased in 2020, whereas O_3 showed an upward trend in clustering, necessitating further explanation. Furthermore, the application of

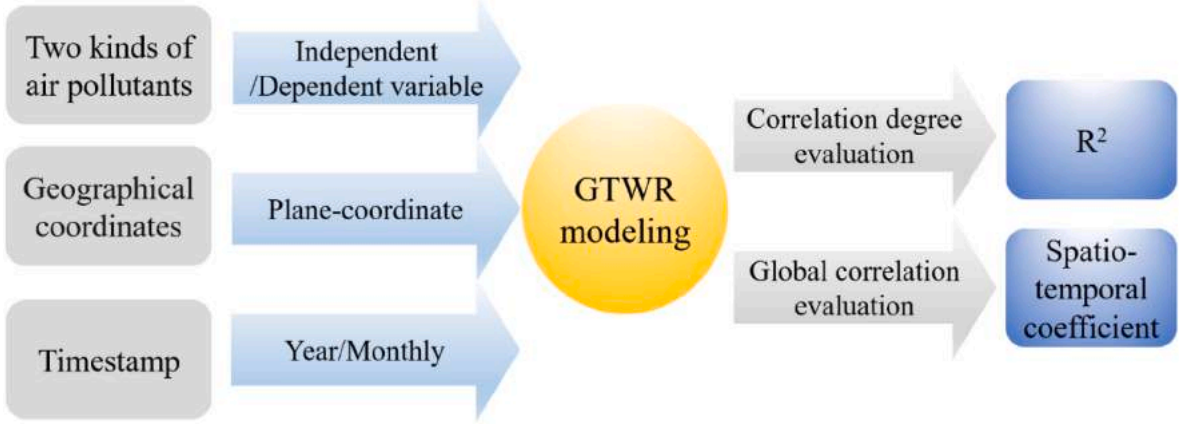

Fig. 3. Implementation process of GTWR model to investigate spatiotemporal correlation.

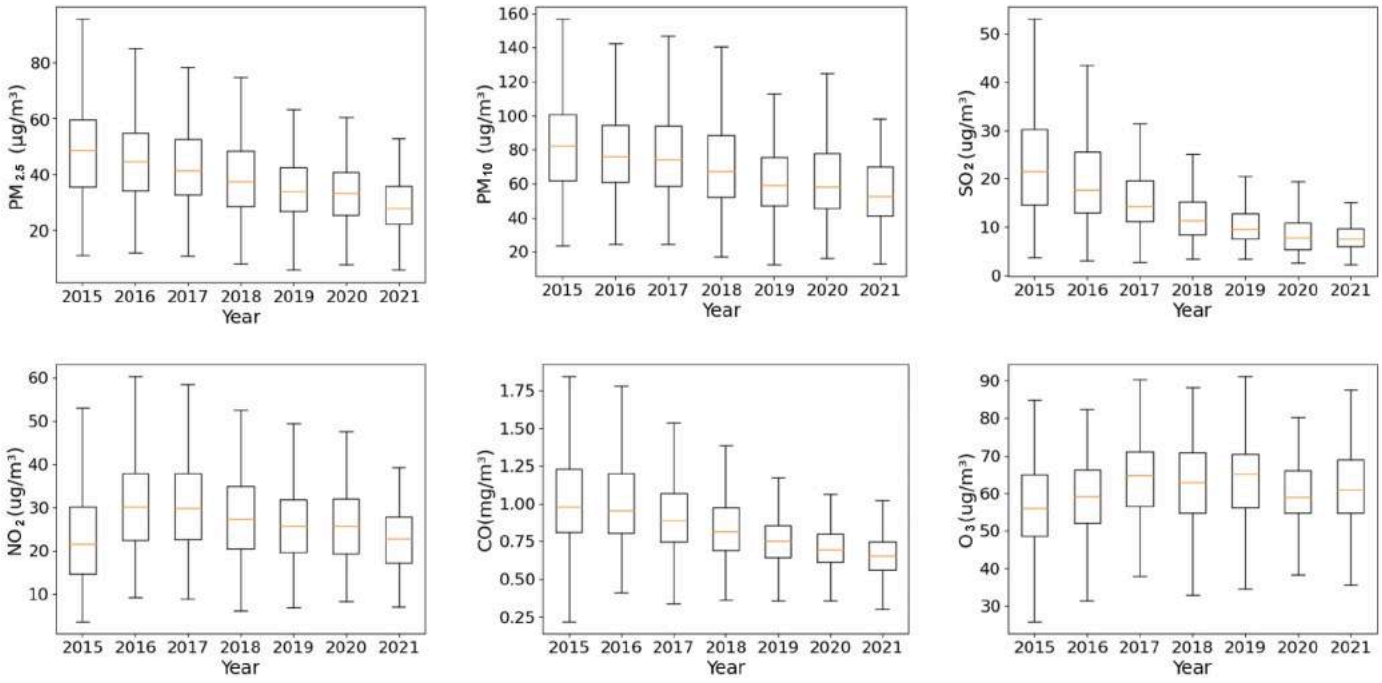

Fig. 4. Comparison of annual trend changes of various pollutants.

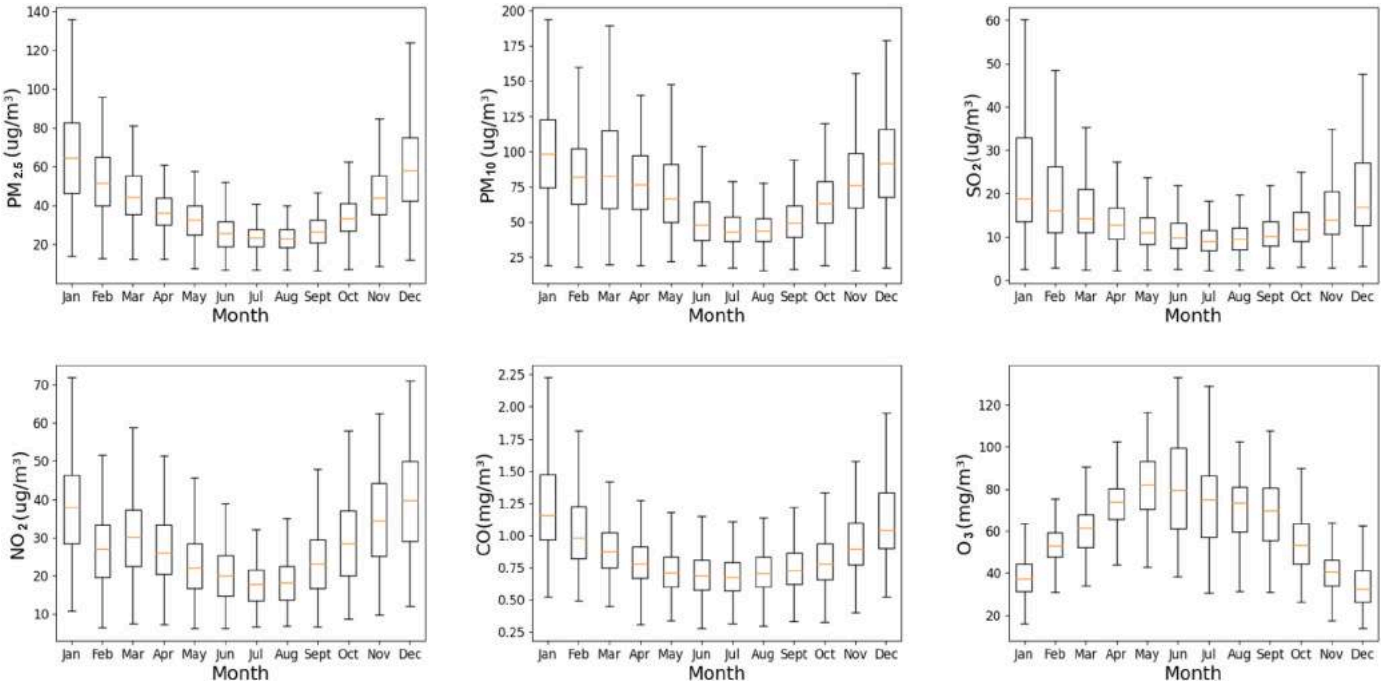

Fig. 5. Comparison of monthly trend changes of various pollutant.

Moran's I statistic reveals notable correlations in the seasonal variations of urban air pollutants (Table 2b). Specifically, the concentration of $PM_{2.5}$, the primary urban air pollutant, exhibits a higher degree of aggregation with values exceeding 0.5, except during spring. Conversely, the concentration of O_3 demonstrates a high level of aggregation during summer, while its aggregation is lowest during winter. Additionally, the aggregation of other pollutants is lower during summer and higher during winter.

Further investigations have revealed geographic concentrations of urban air pollutants. Detailed plots depicting the annual and seasonal mean changes in urban air pollutant concentrations, as well as Local Indicators of Spatial Association (LISA) in China between 2015 and 2021, are presented in Figs. 6–11. The characteristics of annual mean variation indicate that stations with the highest annual concentrations of $PM_{2.5}$ and PM_{10} are predominantly located in North China, followed by Northeast China and Central China. The LISA feature map illustrates a state of High-High (H–H) aggregation, particularly in northern and Central East China (Figs. 6 and 7). This region belongs to the North China Plain, characterized by flat terrain, numerous rivers and lakes, convenient transportation, and economic development, which results in

Table 2
Annual/Seasonal global Moran's I from 2015 to 2021.

Timestamp	$PM_{2.5}$	PM_{10}	SO_2	NO_2	CO	O_3
(a) Year						
2015	0.62	0.61	0.60	0.60	0.51	0.49
2016	0.62	0.61	0.62	0.54	0.52	0.51
2017	0.61	0.59	0.55	0.57	0.49	0.55
2018	0.64	0.62	0.53	0.59	0.50	0.58
2019	0.59	0.58	0.50	0.57	0.47	0.55
2020	0.52	0.61	0.52	0.50	0.50	0.63
2021	0.57	0.44	0.41	0.50	0.38	0.43
(b) Season						
Spring	0.45	0.45	0.53	0.53	0.45	0.46
Summer	0.54	0.42	0.40	0.47	0.45	0.58
Autumn	0.56	0.49	0.51	0.57	0.43	0.53
Winter	0.57	0.54	0.63	0.56	0.45	0.39

relatively intensive human activities. Western Xinjiang is another region with high concentrations of $PM_{2.5}$ and PM_{10}. This area suffers from serious desertification, low vegetation coverage, soil and water loss, and high coarse particle pollutant content (Rupakheti et al., 2021). Conversely, stations with the lowest annual concentrations of $PM_{2.5}$ and PM_{10} are typically located in the Qinghai-Tibet Plateau, South China, and Southwest China. Particularly in the coastal areas of South China, the strong sea breeze in this region has a certain adsorption effect on pollutants. The Pearl River Delta, known for its economic development, has implemented effective control and prevention measures.

In terms of seasonal spatial variation, $PM_{2.5}$ and PM_{10} in western Xinjiang exhibit a low influence with seasonal variation (Figs. 6 and 7). The climate in this region is characterized by fast and erratic changes in spring and short, fast seasons in autumn, with predominantly sunny days, abundant sunshine, dry air, and frequent sandstorms. Regarding spatial concentration, $PM_{2.5}$ shows a significant decrease in summer, autumn, and winter. On the other hand, PM_{10} consistently exhibits a High-High (H–H) aggregation state, with surrounding areas being affected by this H–H aggregation state, displaying a Low-High (L-H) aggregation state.

The highest concentrations of SO_2 and NO_2 have been consistently observed in and around Beijing, Tianjin, and Hebei Province, which constitute a cluster of heavy chemical industries. This area exhibits a High-High (H–H) concentration pattern (Figs. 8 and 9). While particle pollution has been effectively controlled through collaborative efforts, CO concentrations have also been well regulated. Since 2015, the pollution scope has continuously decreased, resulting in significant improvements in the air quality, particularly since 2019 (Fig. 10). The annual peak of O_3 concentration is observed in North China, East China, and Central China, especially in the Beijing-Tianjin-Hebei urban agglomeration. There has been an increasing trend in O_3 concentration from 2017 to 2018 (Fig. 11). During the pandemic period of 2020–2021, the reduction of industrial activities led to a decrease in urban air pollutants and improved visibility. This, in turn, promoted photochemical reactions to some extent, facilitating the formation of O_3. The LISA feature map of O_3 reveals a large and broad High-High (H–H) aggregation area, extending from the densely populated Beijing-Tianjin-Hebei region to the vast and sparsely populated northwest China. The concentrations of urban air pollutants, including $PM_{2.5}$, PM_{10}, SO_2, NO_2, and CO, are significantly influenced by human activities. Liu and Wang conducted a specific investigation on the impact of human activities on cities (Liu and Wang, 2022). Since air pollution exhibits a nonlinear nature, effective management of human activities is crucial for reducing pollutant concentrations. Xue et al. (2022) studied the decrease in urban air pollutants in the North China Plain during 2016–2019, except for O_3, under policy control. This study also found that the concentration of O_3 did not decrease with the reduction in human activities during the COVID-19 pandemic.

During winter, $PM_{2.5}$, PM_{10}, SO_2, NO_2, and CO exhibit high concentrations, particularly in the North China Plain (Figs. 6k to 10k). The most severe pollutants are $PM_{2.5}$ and SO_2, which spread outward from the Beijing-Tianjin-Hebei (BTH) region (Figs. 6 and 8). SO_2 concentration is more pronounced in winter in plain areas such as the Ningxia Plain, the North China Plain, and the Northeast Plain (Fig. 8). In these

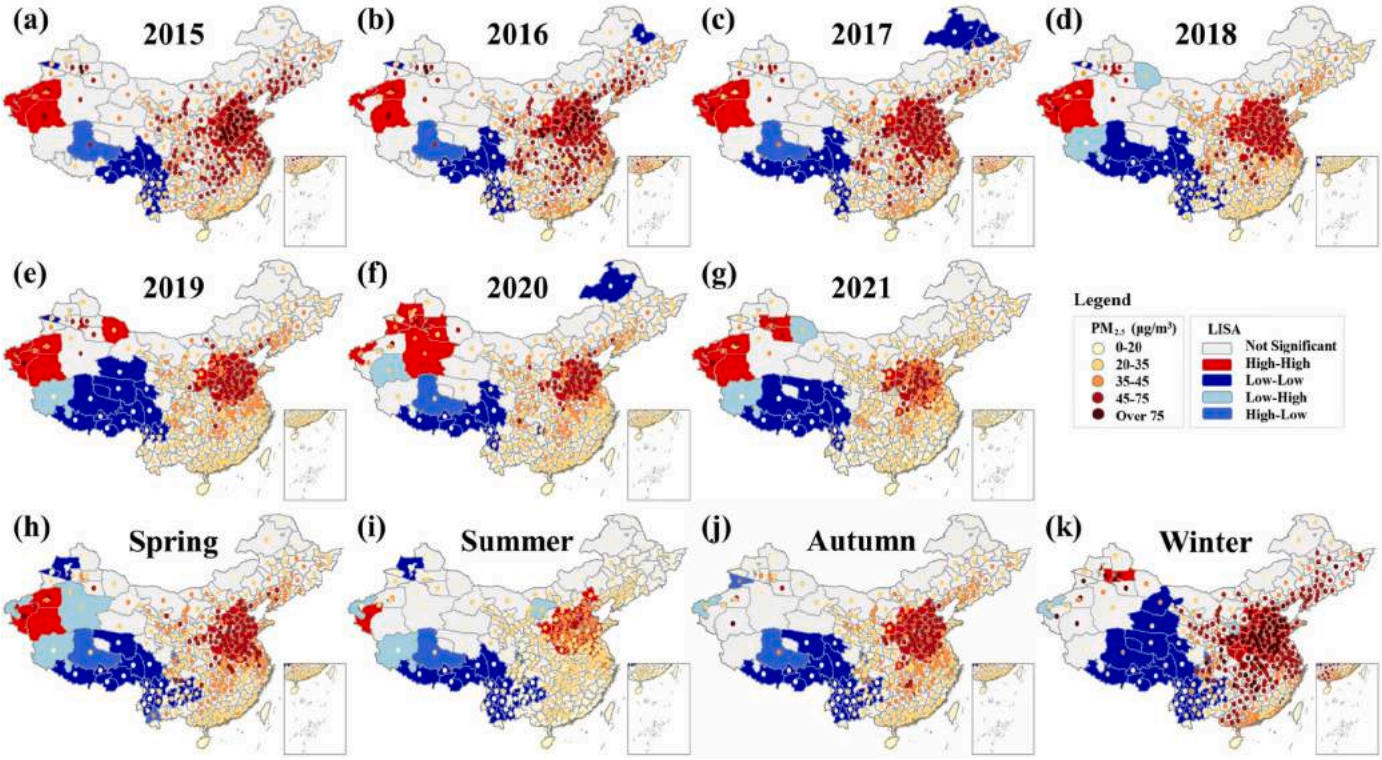

Fig. 6. Annual/seasonal average variations of $PM_{2.5}$ concentrations in China from 2015 to 2021.

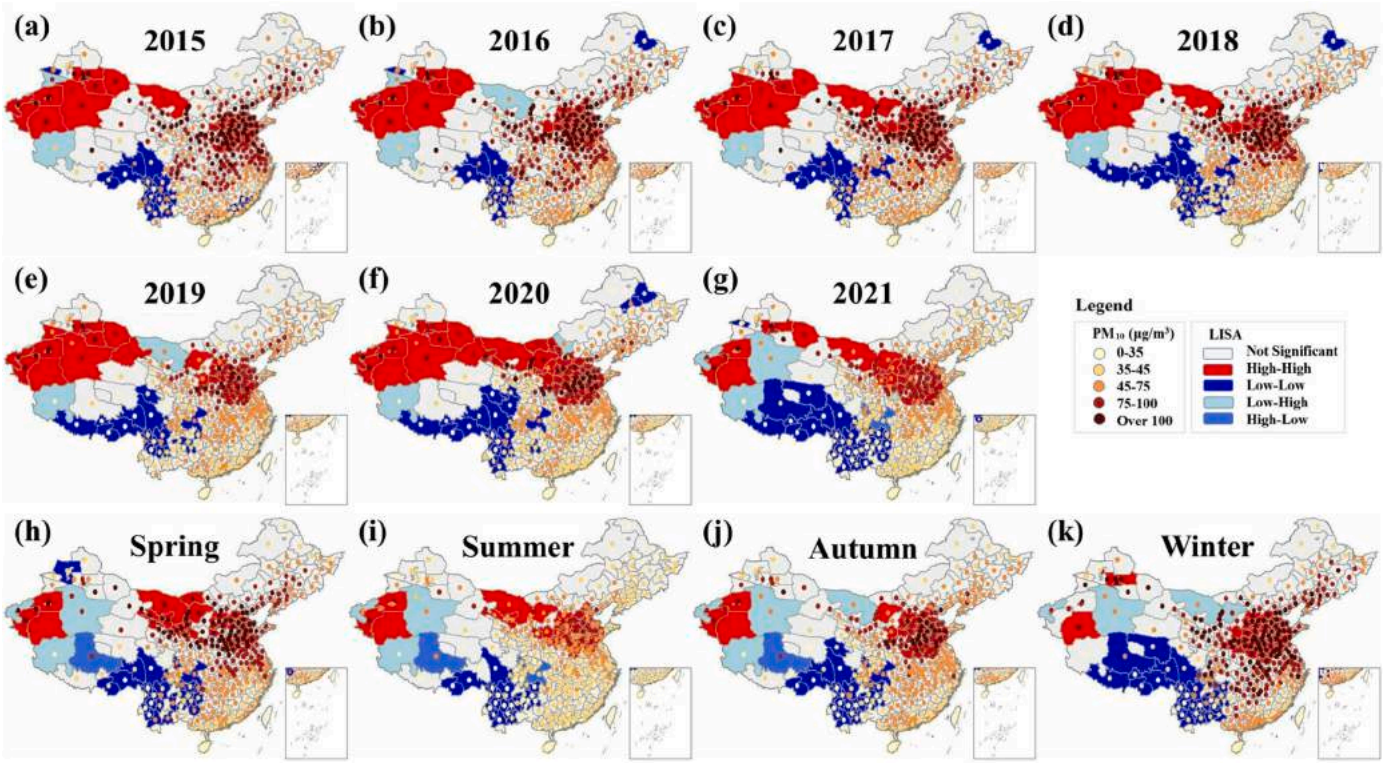

Fig. 7. Annual/seasonal average variations of PM_{10} concentrations in China from 2015 to 2021.

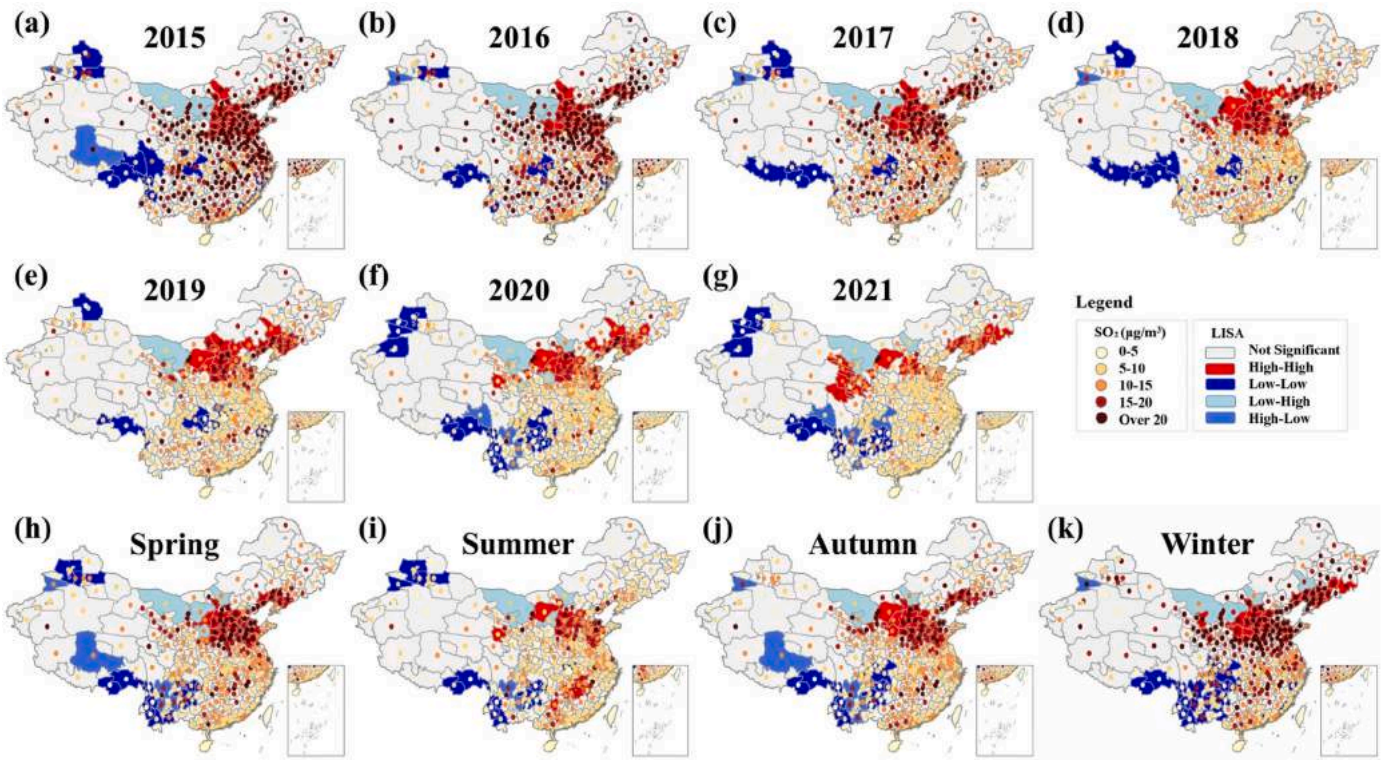

Fig. 8. Annual/seasonal average variations of SO_2 concentrations in China from 2015 to 2021.

plain areas, SO_2 exhibits high pollution levels during winter. The southwest airflow transports various pollutants from Hebei Province to the national plain (Zhao et al., 2022). The persistent pollution in the northwest region throughout the year is attributed to the influence of air masses from the Xinjiang desert region on particle pollution concentration (Turap et al., 2019), as well as secondary strata, biomass and waste combustion, vehicle emissions, crustal minerals, industrial pollution, and coal combustion (Chen et al., 2020). Overall, changes in

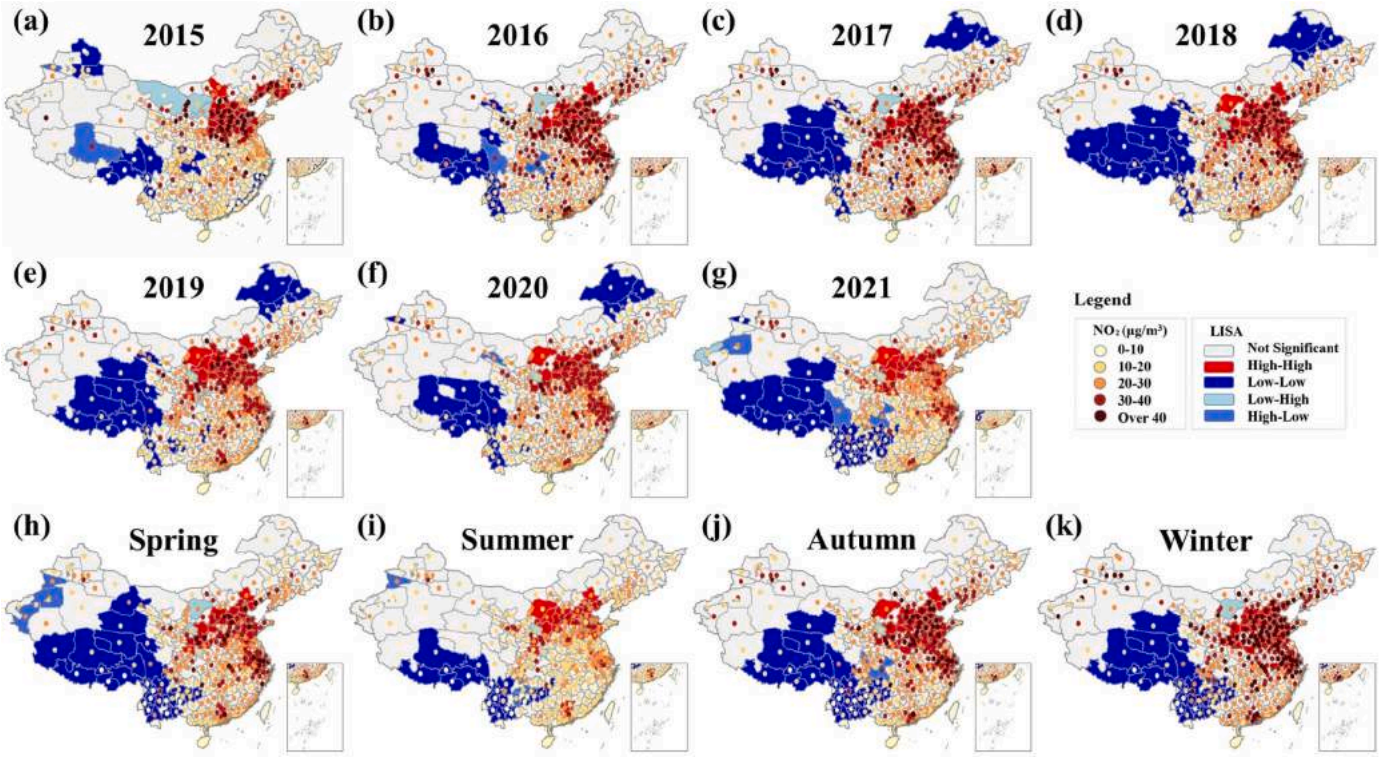

Fig. 9. Annual/seasonal average variations of NO_2 concentrations in China from 2015 to 2021.

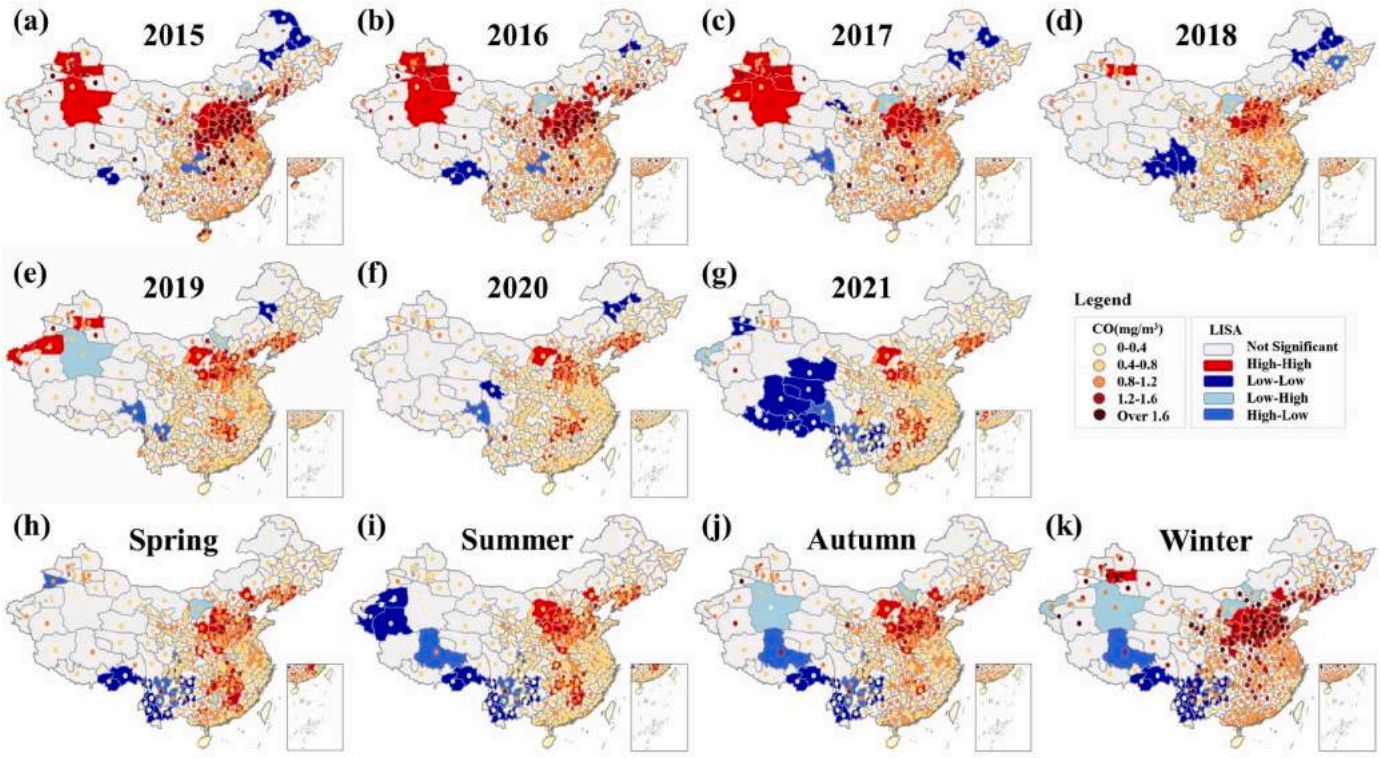

Fig. 10. Annual/seasonal average variations of CO concentrations in China from 2015 to 2021.

pollutant concentration have not led to a shift in the spatial distribution of pollutants.

O_3 concentrations are highest in northern regions during spring and summer, and in southern regions during autumn and winter (Fig. 11). Specifically, O_3 pollution is severe in summer and primarily distributed in Ningxia, Inner Mongolia, and Qinghai. Inner Mongolia experiences a characteristic temperature pattern with a sudden increase in spring, windy weather, a short and hot summer with concentrated precipitation, and a sharp temperature drop and early frost in autumn. Qinghai, located on a plateau with a thin atmosphere and low pressure, has an

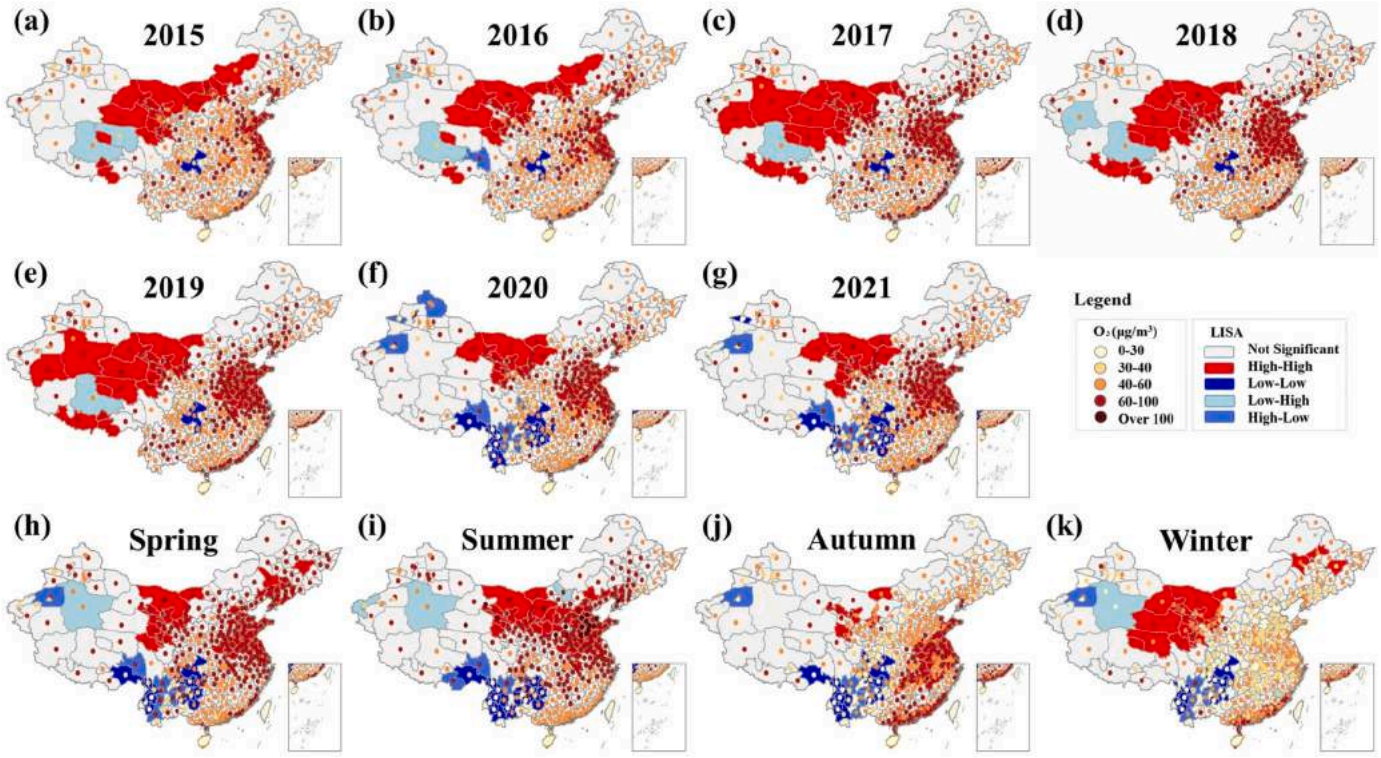

Fig. 11. Annual/seasonal average variations of O_3 concentrations in China from 2015 to 2021.

increased rate of oxygen molecule photolysis, promoting O_3 formation. Although pollutant concentrations generally increase in winter, they gradually decrease with the implementation of clean heating measures and reduced winter heating impacts (Wang et al., 2023). Liu et al. (2023) analyzed prevailing southerly and southeasterly winds in the North China Plain during summer from 2015 to 2020 and found that they intensified O_3 pollution in the northern region. Similarly, prevailing northerly and northwesterly winds during winter intensified O_3 pollution in the southern region, consistent with the findings of this study. During summer, O_3 concentrations are high in Ningxia, Inner Mongolia, and Qinghai, with coal emissions in Ningxia and Shaanxi, vehicle and biomass emissions in Inner Mongolia and Ningxia, and dust emissions in Shaanxi and Henan being the main contributors to pollution (Li et al., 2022). The H–H cluster for O_3 is located in Inner Mongolia and Gansu provinces, and the concentration range shows irregular increases and decreases. The reasons for the increase in O_3 concentrations during summer should be comprehensively considered, including atmospheric vertical movement, chemical reactions, and meteorological conditions (Chen et al., 2023; Zhou et al., 2022).

From 2015 to 2021, there were no significant changes in the spatial pattern of pollutant concentrations. Therefore, it is crucial to continue focusing on key prevention and control measures in high-high concentration areas, such as the Beijing-Tianjin-Hebei (BTH) region and its surrounding cities, as well as cities like Hohhot and Baotou in Inner Mongolia Autonomous Region. As urban air pollutant concentrations and spatial patterns vary with the seasons, it is important to strengthen management measures to reduce emissions from pollution sources during high-pollution seasons and in high-high concentration areas. Preventive measures should also be implemented in low-high concentration areas to improve overall air quality. Based on the analysis above, it is evident that urban air pollutants exhibit strong spatial and temporal correlations. To quantify and compare the degree of correlation, additional spatiotemporal analysis methods are needed to characterize their relationships.

3.3. Spatial and temporal correlation of urban air pollutants

Traditional correlation algorithms, without considering the effects of time and spatial location, have not fully revealed the interrelationships among various pollutants in cities (Kuerban et al., 2020; Zhao et al., 2021). To address this limitation, we employed OLS regression and GWR techniques to investigate spatial correlations. Additionally, we utilized GTWR to examine the influence of spatiotemporal changes, thus establishing the spatiotemporal relationship between pollutants. By comparing the monthly and annual pollutant trend charts (Figs. 4 and 5), we observed a U-shaped pattern in the monthly changes, indicating non-stationary behavior over time compared to the approximately linear trend observed in the annual data. Consequently, we considered the month as a crucial time factor in the GTWR model.

By considering temporal and spatial changes, the GTWR model provided a more comprehensive understanding of pollutant correlations compared to the OLS and GWR models (Fig. 12). Generally, the GTWR model exhibited a higher explanatory power. While both the GTWR model and the Pearson correlation coefficient demonstrated a strong correlation between pollutants, the Pearson correlation coefficient did not account for spatiotemporal factors. In contrast, the GTWR model revealed the influence of spatiotemporal changes on pollutant correlations. While the Pearson correlation coefficient offered a general description of pollutant correlations, the GTWR model enabled further analysis of the degree of correlation between pollutants at the spatiotemporal level.

In our further research, we analyzed the spatiotemporal coefficient changes using the GTWR model. The specific statistical results are presented in Fig. 13, illustrating the variation of coefficients for the six pollutants. The observed range of coefficients indicates continuous changes over time. Notably, we observed significant differences in coefficient ranges between summer and winter. To explore the spatial disparities between these seasons, spatial mapping of the temporal coefficients was conducted for January and July (Fig. 14). The results revealed pronounced differences in the spatial distribution of

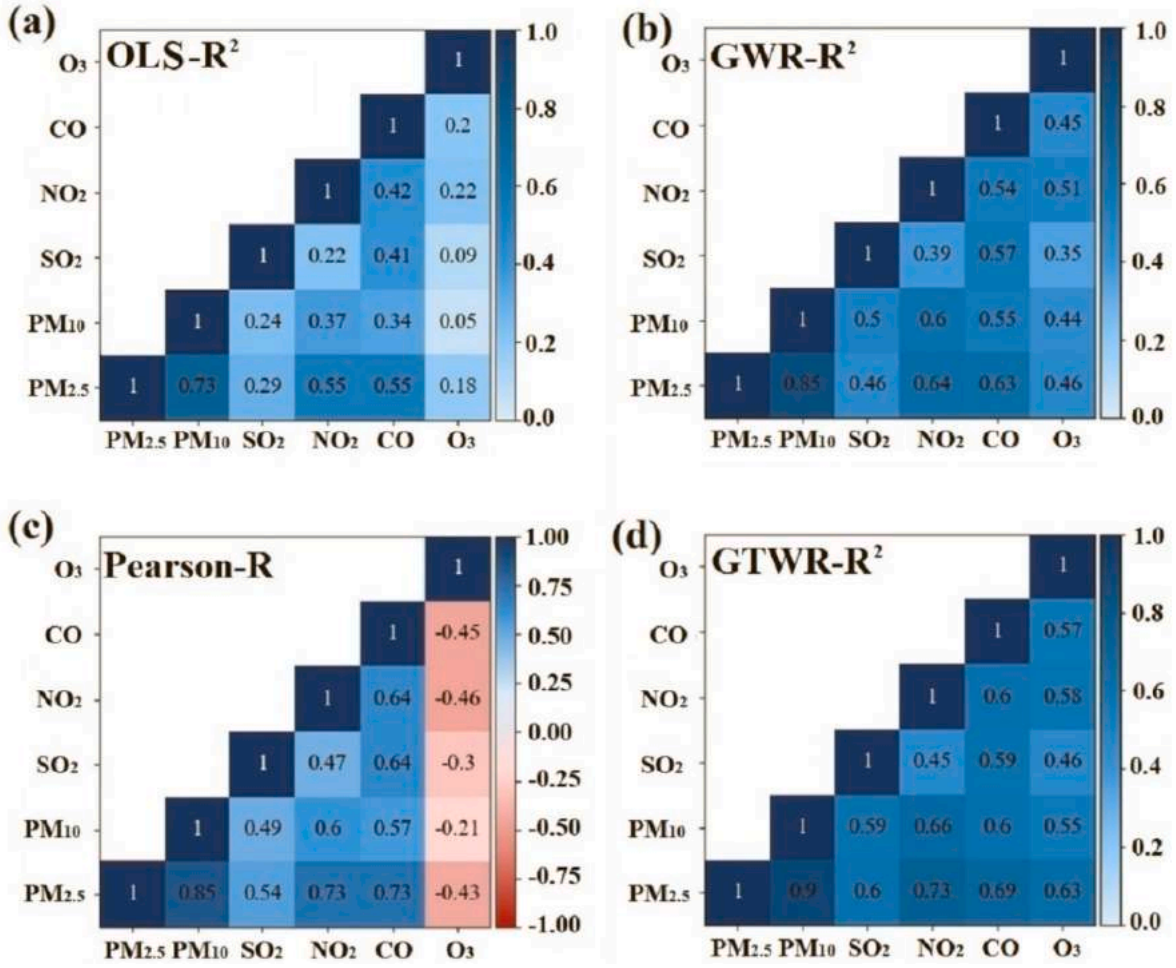

Fig. 12. The correlation of urban air pollutant. (a) represents OLS-R^2. (b) represents GWR-R^2. (c) represents Pearson-R. (d) represents GTWR-$R.^2$.

coefficients between winter and summer. Specifically, the HT line exhibited varying correlation strengths between pollutants, with SO_2, NO_2, and particulate matter showing a stronger correlation. The correlation between CO and other pollutants displayed different intensities along the QH lines, with seasonal changes being less significant. The correlation between O_3 and other pollutants exhibited considerable variation with the seasons. Furthermore, further examination indicated that the coefficients of $PM_{2.5}$, PM_{10}, NO_2, SO_2, and CO were all positive, suggesting a positive correlation among them. In contrast, the coefficients of O_3 and other pollutants were either greater or less than zero. Additionally, the correlation between O_3 and other pollutants varied across different regions from May to August. Consequently, spatial mapping was employed to identify the spatial pattern of O_3 (Fig. 15).

In contrast to previous studies that indicated negative correlations between O_3 and other pollutants (Kuerban et al., 2020; Wang et al., 2020b), our research investigated the spatiotemporal correlation characteristics more comprehensively. Through further exploration of their specific spatial distribution, we found that from May to August, O_3 exhibited a positive correlation with $PM_{2.5}$ and PM_{10} in the southern region of the QH line and Heilongjiang province. Additionally, O_3 showed a positive correlation with SO_2, NO_2, and CO, with the strength of correlation decreasing southward. The positive correlation between O_3 and NO_2 was observed in southern China, while the positive correlation between O_3 and CO and SO_2 was distributed in the middle and southern parts of southern China, encompassing provinces such as Yunnan, Guizhou, Guangxi, and Guangdong. These findings highlight the spatial correlation characteristics between O_3 and other pollutants (Fig. 15). Overall, our use of the GTWR model elucidated the spatiotemporal variations in the correlation between O_3 and other pollutants.

The concentrations of $PM_{2.5}$, PM_{10}, SO_2, NO_2, and CO exhibit similar spatial and temporal variations, as indicated by the high spatiotemporal correlation among them revealed by the GTWR model. These pollutants likely share common driving factors, including terrain-related data such as surface elevation and terrain fluctuation, meteorological data such as precipitation, and human activities characterized by population density and urban green coverage. In 2020, the COVID-19 pandemic had a significant impact on human activities (Zhou et al., 2022), reducing the complexity of factors influencing air quality during the outbreak. Therefore, we used data from January to December 2020 to examine the commonalities of driving factor. Utilizing the GTWR model as a classic spatial regression analysis method, we established the relationship between urban air pollutants and influencing factors. Each individual pollutant served as the dependent variable, and specific independent variables were chosen, as shown in Table 3, with research results presented in Table 4. As can be seen from Fig. 13, most of the changes in the correlation coefficient of pollutants were more obvious in July, where the fluctuations are more obvious, and mapped their coefficients onto a map (Fig. 16). We observed distinct distribution patterns for urban green coverage compared to other driving factors, while the spatial distribution patterns of other driving factors were generally similar. Although O_3 exhibited spatial and temporal differences from other pollutants, its driving factors were similar to those of other pollutants. Consequently, the experimental results confirmed the presence of common driving factors among the six pollutants. The influence of these driving factors on urban air pollutants also demonstrated regional variations along the

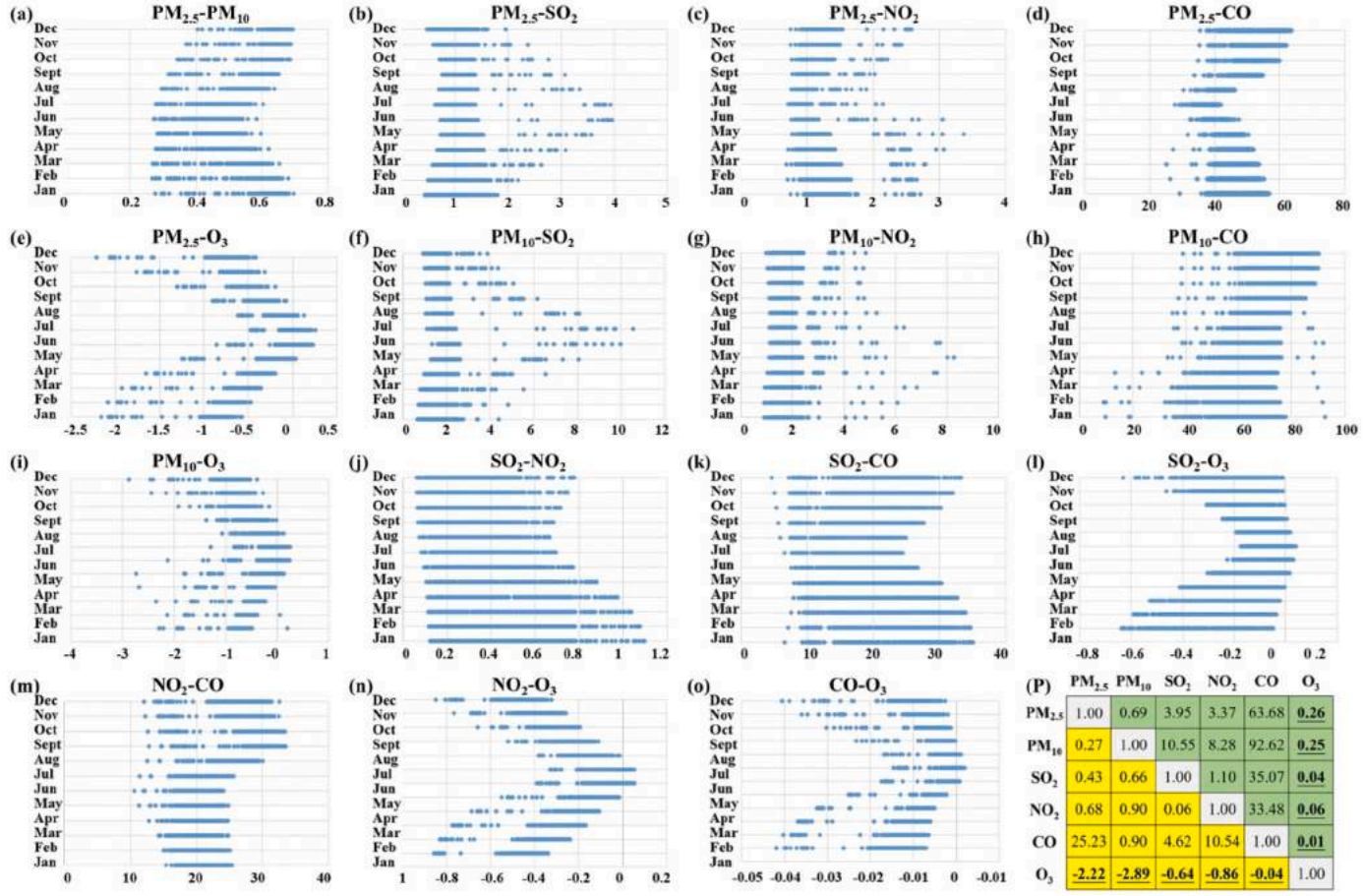

(P)

	$PM_{2.5}$	PM_{10}	SO_2	NO_2	CO	O_3
$PM_{2.5}$	1.00	0.69	3.95	3.37	63.68	0.26
PM_{10}	0.27	1.00	10.55	8.28	92.62	0.25
SO_2	0.43	0.66	1.00	1.10	35.07	0.04
NO_2	0.68	0.90	0.06	1.00	33.48	0.06
CO	25.23	0.90	4.62	10.54	1.00	0.01
O_3	-2.22	-2.89	-0.64	-0.86	-0.04	1.00

Fig. 13. The range of spatial-temporal coefficients(P), with the yellow background indicating the minimum coefficient value and the green background indicating the maximum coefficient value. The scatter plots (a) through (o) represent the monthly spatial-temporal coefficient values for pollutant levels.

HT line and the north-south boundary, known as the QH line, contributing to the spatiotemporal heterogeneity observed in the correlation of urban air pollutants.

3.4. Discussion

These research findings provide profound insights into the issue of air pollution in Chinese cities. Air pollution is a significant environmental problem faced by Chinese cities, as indicated by the research results, particularly concerning $PM_{2.5}$, PM_{10} particles and O_3 (Fig. 6, Figs. 7 and 11). This highlights the urgent need for air quality management amidst rapid urbanization and industrialization.

Seasons and geographic locations have a notable influence on air pollution. The research reveals variations in urban air pollution levels across different seasons and geographic locations. Winter and summer are the seasons with the most severe pollution, and pollution levels also differ among different regions (from Figs. 6–11). Consequently, when formulating air pollution control strategies, it is essential to consider the impact of seasons and geographic factors and implement targeted measures.

Policy governance plays a positive role in addressing air pollution. The research results demonstrate the positive effects of policy governance on improving air pollution in Chinese cities. Concentrations of various pollutants have generally decreased, especially $PM_{2.5}$. However, O_3 concentrations have increased (Wei et al., 2022), possibly due to changes in the generation pathway of O_3 resulting from reduced particulate pollution. This indicates the need for a comprehensive consideration of the interrelationships between different pollutants when addressing air pollution (Figs. 13 and 14).

Air pollution exhibits spatiotemporal heterogeneity. The adoption of the GTWR model in the research reveals spatiotemporal heterogeneity among different pollutants (Fig. 12d). The correlations and spatial distributions of different pollutants are influenced by seasons and geographic locations. This implies that differentiated measures need to be taken based on specific spatiotemporal characteristics when formulating air pollution control strategies.

$PM_{2.5}$, PM_{10}, SO_2, NO_2, and CO exhibit similar spatiotemporal variation patterns and demonstrate high spatiotemporal correlations. The GTWR model was employed for regression analysis, revealing that meteorological data, terrain-related data, and human activities serve as common driving factors for these six pollutants (Fig. 16). While O_3 exhibits distinct spatiotemporal characteristics compared to other pollutants, its spatial driving factors are similar to those of the other pollutants. The spatial distribution pattern of these driving factor coefficients provides an explanation for the spatiotemporal heterogeneity observed in pollutant correlations. However, it is important to note that this study only utilized a single dependent variable for spatial regression modeling, thereby overlooking the interaction among the six pollutants. As a result, future research should analyze these six pollutants as a collective entity (Chen et al., 2022a), considering their interconnectedness and spatiotemporal differences.

Despite having obtained relatively accurate ground data from CNEMC, there are still some missing data in certain regions. As the GTWR model requires continuous regional data, we plan to further improve the dataset by incorporating remote sensing data and utilizing more mature data imputation methods for processing (Tharzeen et al., 2023), and refining the time scale to daily or hourly units. However, this will pose some challenges for the regression model in handling big data

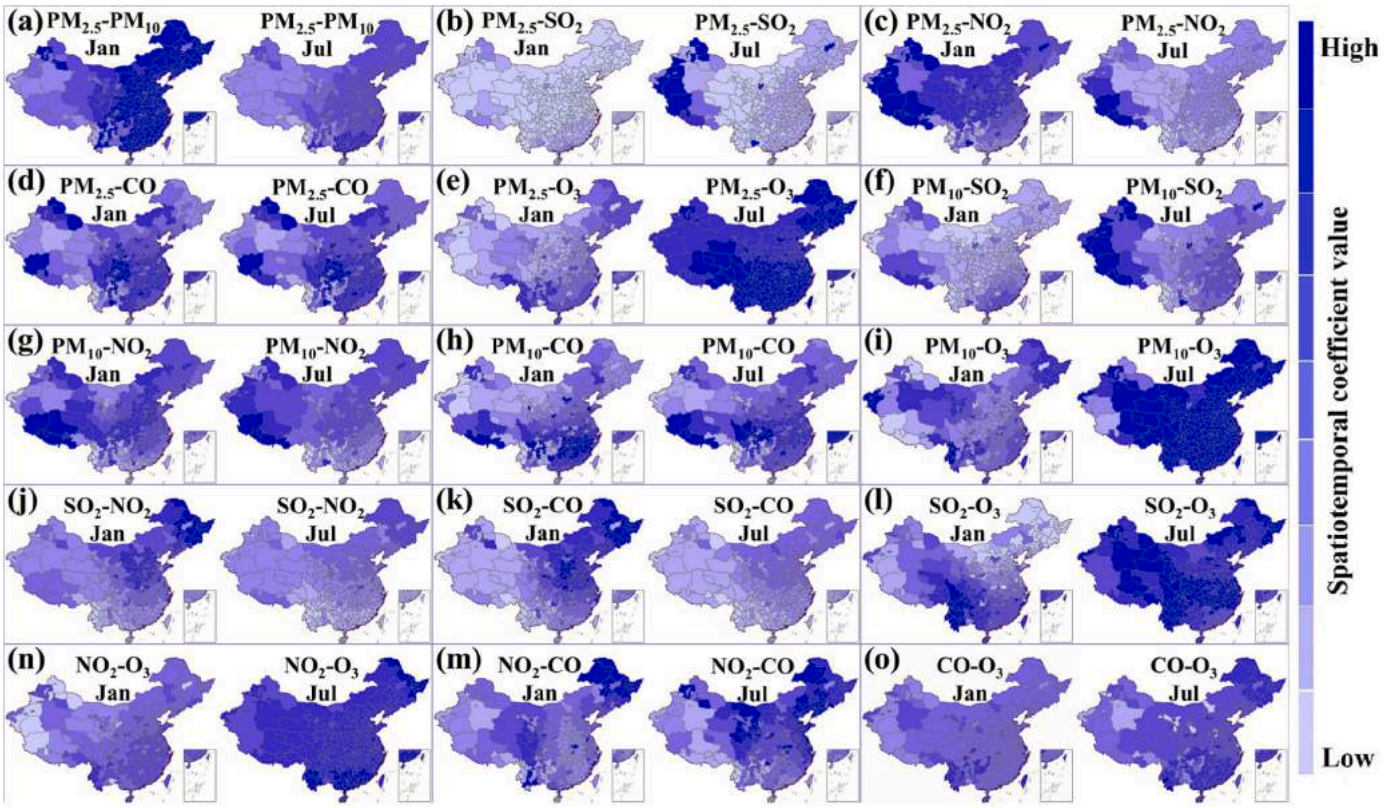

Fig. 14. Spatial mapping of January (winter) and July (summer) spatiotemporal coefficients.

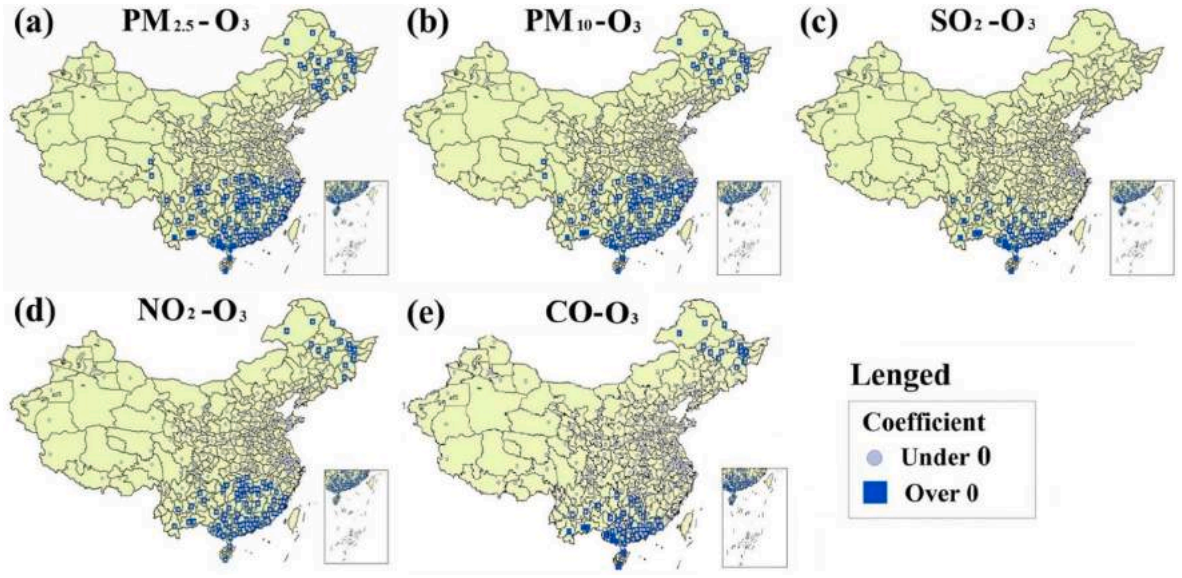

Fig. 15. Spatial distribution of O_3 and other pollutants from May to August.

Table 3
Definitions of the independent variables.

Variables	Abbr.	Min	Max	Std.	Mean
Terrain fluctuation	TF	0.001	5.791	±1.157	0.940
Surface elevation	DEM	2.853	5044.380	±899.269	637.953
Urban Green Coverage	UGC	0.001	0.995	±0.219	0.530
Population Density	PD	0.263	8283.560	±634.070	422.741
Precipitation Total	PT	4.814	807.979	±146.883	177.771

Table 4
Modeling the relationship between pollutants and driving factors.

Model	R^2	Bandwidth	Alcc	CV
GTWR-$PM_{2.5}$	0.81	207.42	3039.42	230.39
GTWR-PM_{10}	0.85	249.55	3392.42	1134.05
GTWR-SO_2	0.71	262.57	2819.96	229.43
GTWR-NO_2	0.76	273.11	2430.69	71.11
GTWR-CO	0.65	294.17	68.09	0.08
GTWR-O_3	0.83	212.89	2538.12	212.89

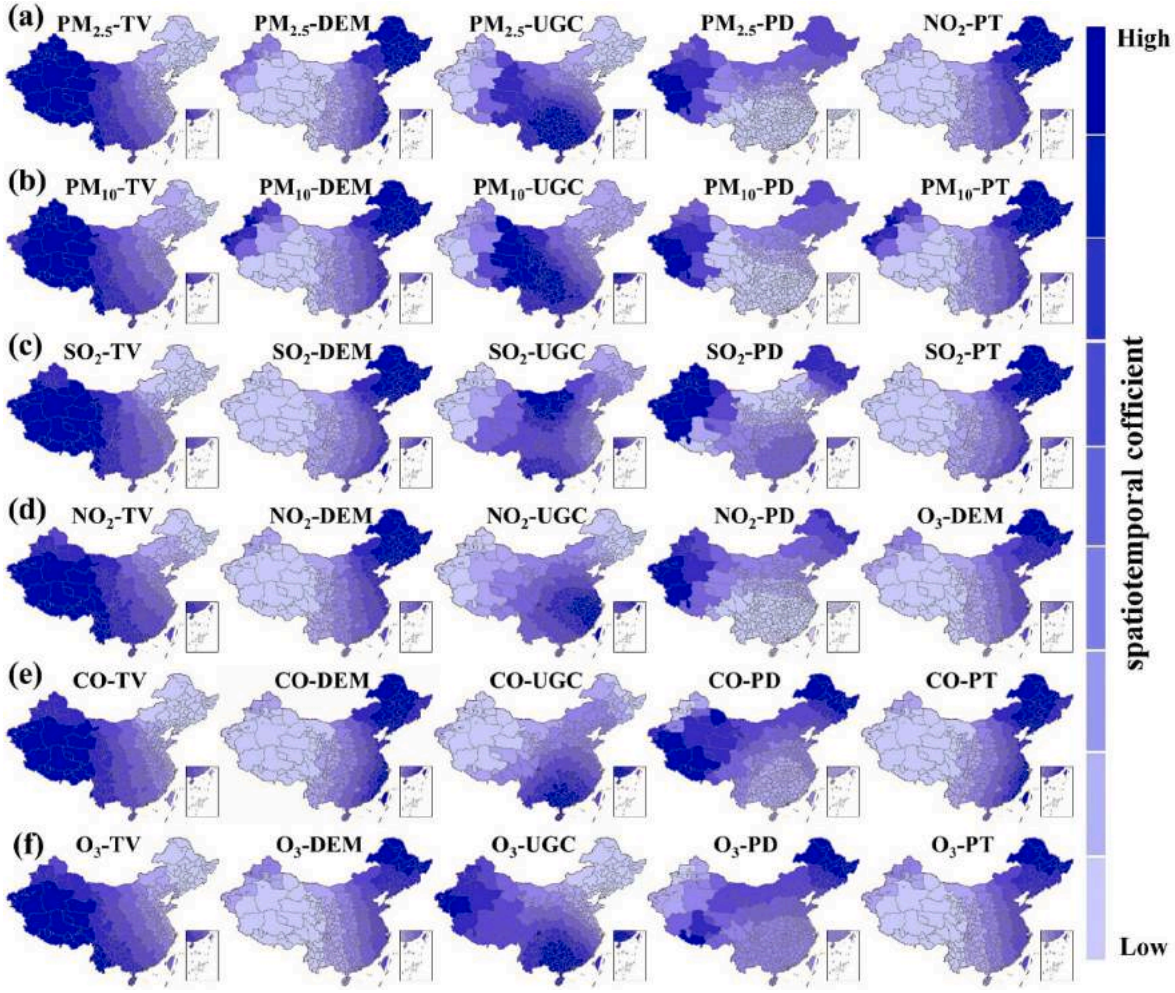

Fig. 16. Spatial mapping of the coefficient for July 2020.

(Wang et al., 2020a; Yang et al., 2023). In future studies, we will aim to further optimize the GTWR model to address these issues.

4. Conclusion

In conclusion, a comprehensive analysis of the spatial distribution of environmental pollutants in Chinese urban clusters has been conducted in this study. The regression model has revealed the interrelationships among air pollutants in China's national-level cities. Compared to traditional correlation algorithms, the GTWR model, which takes into account the influence of time and spatial location, provides a more comprehensive understanding of these interrelationships and aids in effective pollution control. In particular, we have identified significant spatiotemporal heterogeneity between O_3 and other pollutants, as well as potential relationships among the six types of pollutants. These spatiotemporal relationships are significantly associated with terrain fluctuation, surface elevation, urban green coverage, population density and precipitation total, providing regional reference for pollution control planning in different areas. Based on the preliminary exploration of the spatiotemporal correlation of pollutants in this study in the future, by enhancing the computational power of the GTWR model, improving the temporal resolution, and incorporating the inherent relationships among pollutants, we can generate more accurate and up-to-date information.

Credit author statement

Conceptualization, C.Y. and Y.Y.; writing—original draft preparation, C.Y., Y.Q.; supervision, Y.Y., H.K.; writing—review and editing, H. H., Y.Y. and S.X.; funding acquisition, S.X. and Y.Z.; Data collection, L.J. and Y.X. All authors have read and approved the final manuscript.

Declaration of competing interest

The authors declare that they have no known competing financial interests or personal relationships that could have appeared to influence the work reported in this paper.

Acknowledgments

This research was funded by the National Natural Science Foundation of China, grant number 42001343; and the National Natural Science Foundation of China, grant number 42071384.

References

Brunsdon, C., et al., 1996. Geographically weighted regression: a method for exploring spatial nonstationarity. Geogr. Anal. 28, 281–298.
Cai, J.Z., et al., 2017. Analyzing the characteristics of soil moisture using GLDAS data: A case study in Eastern China. Applied Sciences-Basel vol. 7.
Cao, B., et al., 2020. Factors influencing the boundary layer height and their relationship with air quality in the Sichuan Basin, China. Sci. Total Environ. 727, 138584.
Chen, J., et al., 2020. Characteristics and sources analysis of PM2.5 in a major industrial city of Northern Xinjiang, China. SN Applied Sci. vol. 2.

Chen, S., et al., 2023. Diagnosis of photochemical O(3) production of urban plumes in summer via developing the real-field IRs of VOCs: a case study in Beijing of China. Environ. Pollut. 318, 120836.
Chen, V.Y.-J., et al., 2022a. Geographically weighted regression modeling for multiple outcomes. Ann. Assoc. Am. Geogr. 112, 1278–1295.
Chen, Y., et al., 2022b. The relationship between air quality and MODIS aerosol optical depth in major cities of the Yangtze River Delta. Chemosphere 308, 136301.
Chu, H.-J., et al., 2015. Modeling the spatio-temporal heterogeneity in the PM10-PM2.5 relationship. Atmos. Environ. 102, 176–182.
Comber, A., et al., 2023. A route map for successful applications of geographically weighted regression. Geogr. Anal. 55, 155–178.
Filonchyk, M., et al., 2018. Temporal and spatial variation of particulate matter and its correlation with other criteria of air pollutants in Lanzhou, China, in spring-summer periods. Atmos. Pollut. Res. 9, 1100–1110.
Guan, M., et al., 2019a. An effective method for submarine buried pipeline detection via multi-sensor data fusion. IEEE Access 7, 125300–125309.
Guan, M., et al., 2019b. A method of establishing an instantaneous water level model for tide correction. Ocean Eng. 171, 324–331.
Guo, Y., et al., 2017. Estimating ground-level PM2.5 concentrations in Beijing using a satellite-based geographically and temporally weighted regression model. Rem. Sens. Environ. 198, 140–149.
Han, X., et al., 2020. Heterogeneity of influential factors across the entire air quality spectrum in Chinese cities: a spatial quantile regression analysis. Environ. Pollut. 262.
He, Q., Huang, B., 2018. Satellite-based mapping of daily high-resolution ground PM2.5 in China via space-time regression modeling. Rem. Sens. Environ. 206, 72–83.
He, S., et al., 2022. RSI-Net: two-stream deep neural network for remote sensing images-based semantic segmentation. IEEE Access 10, 34858–34871.
Huang, B., et al., 2010. Geographically and temporally weighted regression for modeling spatio-temporal variation in house prices. Int. J. Geogr. Inf. Sci. 24, 383–401.
Jiang, F., et al., 2023. Spatio-temporal evolution and influencing factors of synergizing the reduction of pollution and carbon emissions - utilizing multi-source remote sensing data and GTWR model. Environ. Res. 229, 115775.
Karimian, H., et al., 2019. Spatio-temporal variation of wind influence on distribution of fine particulate matter and its precursor gases. Atmos. Pollut. Res. 10, 53–64.
Karimian, H., et al., 2017. Daily estimation of fine particulate matter mass concentration through satellite based aerosol optical depth. ISPRS Annals Photogrammet. Remote Sens. Spat. Inf. Sci. IV-4/W2, 175–181.
Karimian, H., et al., 2023. Evaluation of different machine learning approaches and aerosol optical depth in PM(2.5) prediction. Environ. Res. 216, 114465.
Kong, L., et al., 2021. A 6-year-long (2013–2018) high-resolution air quality reanalysis dataset in China based on the assimilation of surface observations from CNEMC. Earth Syst. Sci. Data 13, 529–570.
Kuerban, M., et al., 2020. Spatio-temporal patterns of air pollution in China from 2015 to 2018 and implications for health risks. Environ. Pollut. 258, 113659.
Li, X.F., et al., 2022. Carbonaceous aerosols in Lvliang, China: seasonal variation, spatial distribution and source apportionment. Environ. Chem. 19, 90–99.
Liao, H., et al., 2022. Acute effects of ambient air pollution exposure on lung function in the elderly in Hangzhou, China. Int. J. Environ. Health Res. 1–11.
Liu, L., Wang, Q., 2022. Is the effect of human activity on air pollution linear or nonlinear? Evidence from Wuhan, China, under the COVID-19 lockdown. Cities 127.
Liu, S., et al., 2023. Meteorological mechanisms of regional PM2.5 and O3 transport in the North China Plain driven by the East Asian monsoon. Atmos. Pollut. Res. 14.
Liu, Y., et al., 2020. The impact of different mapping function models and meteorological parameter calculation methods on the calculation results of single-frequency precise point positioning with increased tropospheric gradient. Math. Probl. Eng. 2020, 1–12.
Mariscal-Aguilar, P., et al., 2023. Relationship between air pollution exposure and the progression of idiopathic pulmonary fibrosis in Madrid: Chronic respiratory failure, hospitalizations, and mortality. A retrospective study. Front. Public Health 11.
McKeon, T.P., et al., 2022. Air pollution and lung cancer survival in Pennsylvania. Lung Cancer 170, 65–73.
Ouyang, H.L., et al., 2022. Toward better and healthier air quality: implementation of WHO 2021 global air quality guidelines in Asia. Bull. Am. Meteorol. Soc. 103, E1696–E1703.
Pompilio, A., Di Bonaventura, G., 2020. Ambient air pollution and respiratory bacterial infections, a troubling association: epidemiology, underlying mechanisms, and future challenges. Crit. Rev. Microbiol. 46, 600–630.
Qiu, Z., et al., 2020. Dam structure deformation monitoring by GB-InSAR approach. IEEE Access 8, 123287–123296.
Rupakheti, D., et al., 2021. Spatio-temporal characteristics of air pollutants over Xinjiang, northwestern China. Environ. Pollut. 268, 115907.
Ryter, S.W., et al., 2018. Carbon monoxide in lung cell physiology and disease. Am. J. Physiol. Cell Physiol. 314, C211–C227.
Shen, Y., et al., 2022. Europe-wide air pollution modeling from 2000 to 2019 using geographically weighted regression. Environ. Int. 168, 107485.
Tan, J., et al., 2022. A new ensemble spatio-temporal PM2.5 prediction method based on graph attention recursive networks and reinforcement learning. Chaos, Solit. Fractals 162.
Tharzeen, A., et al., 2023. A General Spatiotemporal Imputation Framework for Missing Sensor Data. 2023 IEEE Conference on Artificial Intelligence (CAI), pp. 55–58.
Turap, Y., et al., 2019. Temporal distribution and source apportionment of PM2.5 chemical composition in Xinjiang, NW-China. Atmos. Res. 218, 257–268.
Wang, D., et al., 2020a. A CUDA-based parallel geographically weighted regression for large-scale geographic data. ISPRS Int. J. Geo-Inf. 9.
Wang, J., et al., 2023. The diminishing effects of winter heating on air quality in northern China. J. Environ. Manag. 325, 116536.
Wang, Y., et al., 2022a. Analysis of spatio-temporal distribution characteristics and socioeconomic drivers of urban air quality in China. Chemosphere 291, 132799.
Wang, Y., et al., 2020b. Spatio-temporal distribution of six pollutants and potential sources in the Hexi Corridor, Northwest China. Environ. Monit. Assess. 192, 624.
Wang, Z., et al., 2022b. Geographical and temporal weighted regression model and its application in epidemiology: a review. Zhongguo xue xi chong bing fang zhi za zhi = Chinese journal of schistosomiasis control 35, 199–205.
Wang, Z.Y., et al., 2021. Spatial and temporal characteristics of environmental air quality and its relationship with seasonal climatic conditions in eastern China during 2015-2018. Int. J. Environ. Res. Publ. Health 18.
Wei, J., et al., 2022. Full-coverage Mapping and Spatiotemporal Variations of Ground-Level Ozone (O3) Pollution from 2013 to 2020 across China. Remote Sensing of Environment, p. 270.
Xu, S., et al., 2023. Spatio-temporal effects of regional resilience construction on carbon emissions: evidence from 30 Chinese provinces. Sci. Total Environ. 887, 164109.
Xue, Y.G., et al., 2022. Air pollution: a culprit of lung cancer. J. Hazard Mater. 434.
Yang, X., et al., 2023. A new algorithm for large-scale geographically weighted regression with K-nearest neighbors. ISPRS Int. J. Geo-Inf. 12.
Zhao, C., et al., 2021. Spatio-temporal analysis of urban air pollutants throughout China during 2014-2019. Air Qual Atmos Health 14, 1619–1632.
Zhao, H., et al., 2022. Effects of different aerosols on the air pollution and their relationship with meteorological parameters in North China plain. Front. Environ. Sci. 10.
Zhou, Y., et al., 2022. Summer ozone pollution in China affected by the intensity of Asian monsoon systems. Sci. Total Environ. 849.